

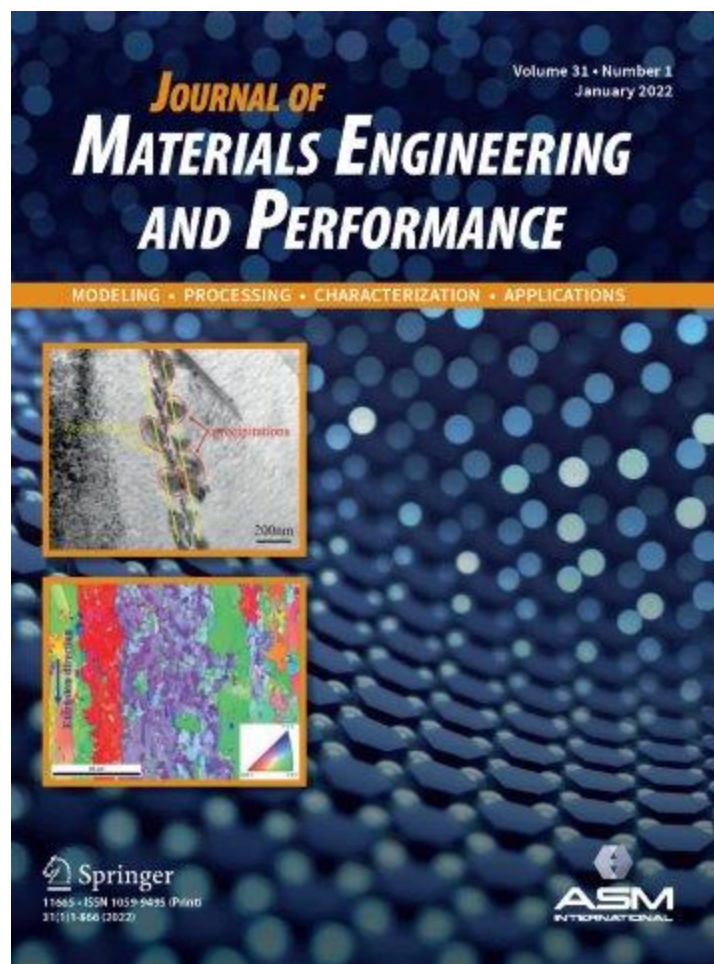


Title	Antibacterial Cu-Doped HA/TiO ₂ Bioactive Ceramic Composite Coating with Enhanced Adhesion on Pure Ti
Author(s)	Yang, Jiawei; Li, Qiang; Li, Junjie et al.
Citation	Journal of Materials Engineering and Performance. 2022, 32(14), p. 6151-6159
Version Type	AM
URL	https://hdl.handle.net/11094/89906
rights	
Note	

The University of Osaka Institutional Knowledge Archive : OUKA

<https://ir.library.osaka-u.ac.jp/>

The University of Osaka



Antibacterial Cu-doped HA/TiO₂ bioactive ceramic composite coating with enhanced adhesion on pure Ti

Journal:	<i>Journal of Materials Engineering and Performance</i>
Manuscript ID	JMEP-22-01-26752.R2
Manuscript Type:	Technical Article
Date Submitted by the Author:	11-Aug-2022
Complete List of Authors:	<p>Yang, Jiawei; University of Shanghai for Science and Technology</p> <p>Li, Qiang;</p> <p>Li, Qiang; University of Shanghai for Science and Technology; Shanghai Engineering Research Center of High-Performance Medical Device Materials</p> <p>Li, Junjie; Xinjiang Technical Institute of Physics and Chemistry, CAS Key Laboratory of Functional Materials and Devices for Special Environments</p> <p>Yang, Jinshuai; University of Shanghai for Science and Technology</p> <p>Zhang, Ran; University of Shanghai for Science and Technology, School of Mechanical Engineering</p>

	Niinomi, Mitsuo; University of Shanghai for Science and Technology; Tohoku University; Osaka University; Meijo University, Department of Materials Science and Engineering; Kansai University Nakano, Takayoshi; Osaka Univ, Division of Materials & Manufacturing Science, Graduate School of Engineering
Keywords:	TiO2 nanopore, electrochemical deposition, Cu-doped hydroxyapatite coating, adhesion, antibacterial properties

SCHOLARONE™
Manuscripts

Dear Editors,

We thank you very much for giving us an opportunity to revise our manuscript. We appreciate editors and reviewers for their positive and constructive comments and suggestions on our manuscript.

We have studied reviewers' comments carefully, and tried our best to revise our manuscript according to the comments. For English, the manuscript is finally revised and polished by a native speaker from an institution named "Editage". Two versions with and without revising trace are both submitted to the journal. Please find our responses to the comments, which we sincerely hope will be up to the satisfaction of the reviewers.

Thank you and best regards!

Yours sincerely,

Qiang Li

Responses to reviewers' comments

We would like to express great appreciation to reviewers for the comments on the manuscript. The main corrections in the manuscript and the responds to the reviewer's comments are as following:

Reviewer(s)' Comments to Author:

Based on our research experience in the field of electrodeposited HA coatings, we may want to recommend the editor to REJECT this paper. The authors prepared CuHA/TiO₂ composite coatings on Ti alloy, but the related characterization does not fully prove the successful synthesis of HA coatings.

Response: Thank you very much for your comment. We know that many studies have been carried out on preparing HA coatings. In this manuscript, we focus on Cu-doping, adhesion, antibacterial property and cytotoxicity. Our results suggest that the Cu-doped composite coatings show enhance adhesion, good antibacterial properties and non-cytotoxicity. Additionally, we will do further study on the better synthesis of Cu-doped HA coatings for biomedical applications.

Specific comments are as follows:

This work reported the preparation and characterizations of TiO₂/ZrO₂ composite PEO coatings on Titanium. The comments on the paper are given as follows.

Response: Thank you very much for your comment. We have revised the manuscript carefully. We hope current revision can satisfy the requirement of publication.

1. Several characteristic peaks of HA from XRD pattern Figure 5 do not prove the formation of HA, and the synthesis may also be other phases of calcium phosphate. This conclusion is easily obtained by comparing with the diffraction file #09-0432 of HA. Thus, we suspect that the authors did not succeed in the electrodeposition synthesis of high purity HA, which may require the authors to optimize the

parameters of electrodeposition to obtain. This still needs a lot of work.

Response: Thank you very much for your comment. According to our previous research (<https://doi.org/10.2320/matertrans.MT-M2021005>), The Cu-doped HA coatings are calcium phosphate coatings based on HA. This manuscript is the preliminary result of our preparation of Cu-doped HA coatings, the purpose is to improve the adhesion of the coatings. We will continue to optimize the parameters and improve the purity of HA in the future. The fabricated CuHA/TiO₂ coatings exhibited high biocompatibility, and promoted the proliferation of MC3T3-E1 cells.

2. Page3 Line44, the authors point out that the disadvantage of HA coatings prepared by electrodeposition is their weak crystallinity. However, this is actually inaccurate. It has been shown that the addition of a certain concentration of hydrogen peroxide to the electrodeposition solution increases the crystallinity of the coating (Doi: 10.1016/j.matlet.2019.126989). The authors should also calculate the crystallinity of HA using Jade software in the subsequent XRD analysis and discussion. The authors need to explain whether titanium dioxide nanopores have any effect on enhancing the crystallinity of HA electrodeposition, which requires additional relevant XRD analysis.

Response: Thank you very much for your comment. The corresponding content has been added. Please see the revised manuscript.

3. Page6 Line10, please add more details of the electrodeposition experiment, such as the distance between cathodes and anodes, the type of electrodeposition equipment

Response: Thank you very much for your comment. The corresponding content has been added. Please see the revised manuscript.

4. The amount of copper doping has a significant effect on the antimicrobial and cytotoxic properties of the coating, and the authors should test the rate and amount of copper ions released in the SBF using ICP to prove “In this study, the

Cu content is maintained at a relatively low level by adjusting the deposition time (Page13 Line50)”.

Response: Thank you very much for your comment. Due to COVID-19, We are currently unable to perform ion release tests. According to our previous research, the quantity of Cu²⁺ release is 0.157 mg/L, which is significantly lower than 9 m g/L (<https://doi.org/10.1002/adhm.202000681>). This finding indicated no cytotoxic effect on MC3T3-E1 cells. We apply for further modification if ion release test is required.

Other minor questions:

1. Page6 Line8, the increase in solution conductivity is mainly attributed to sodium chloride, and the authors' expression is easily misunderstood.

Response: Thank you very much for your comment. The sentence has been modified, please see the revised manuscript.

2. Page8 Line44, are→were, the author wrote the paper in a confusing tense in the analysis and discussion section.

Response: Thank you very much for your comment. The tense has been modified, please see the revised manuscript.

3. “dope” and “substitute” are used to describe the combination of copper and HA in a very different way, and the authors' expression in this paper is confusing. Please strictly distinguish the meaning of these two verbs.

Response: Thank you very much for your comment. The expression has been unified, please see the revised manuscript.

Antibacterial Cu-doped HA/TiO₂ bioactive ceramic composite coating with enhanced adhesion on pure Ti

Jiawei Yang ¹, Qiang Li ^{1,2, *}, Junjie Li ³, Jinshuai Yang ¹, Ran Zhang ¹,

Mitsuo Niinomi ^{1,4,5,6,7 *}, Takayoshi Nakano ⁵

1. School of Mechanical Engineering, University of Shanghai for Science and Technology, Shanghai 200093, P. R. China

2. Shanghai Engineering Research Center of High-Performance Medical Device Materials, Shanghai 200093, P. R. China

3. CAS Key Laboratory of Functional Materials and Devices for Special Environments, Xinjiang Technical Institute of Physics & Chemistry, CAS; Xinjiang Key Laboratory of Electronic Information Materials and Devices, 40-1 South Beijing road, Urumqi 830011, P. R. China

4. Institute for Materials Research, Tohoku University, 2-1-1, Katahira, Aoba-ku, Sendai 980-8577, Japan

5. Division of Materials and Manufacturing Science, Graduate School of Engineering, Osaka University, 2-1, Yamada-Oka, Suita, Osaka 565-0871, Japan

6. Department of Materials Science and Engineering, Graduate School of Science and Technology, Meijo University, 1-501, Shiogamaguchi, Tempaku-ku, Nagoya 468-8502, Japan

7. Faculty of Chemistry, Materials and Bioengineering, Kansai University, Osaka 564-8680, Japan

* Corresponding authors:

Dr. Qiang Li, E-mail addresses: jxli@tju.edu.cn & liqiang@usst.edu.cn

Prof. Mitsuo Niinomi, E-mail address: niinomi@imr.tohoku.ac.jp

1
2
3
4
5
6
7
8
9
10
11
12
13
14
15
16
17
18
19
20
21
22
23
24
25
26
27
28
29
30
31
32
33
34
35
36
37
38
39
40
41
42
43
44
45
46
47
48
49
50
51
52
53
54
55
56
57
58
59
60

Abstract

Cu-doped hydroxyapatite (HA)/TiO₂ (CuHA/TiO₂) bioactive ceramic composite coatings were prepared on Ti surfaces using an electrochemical method to enhance their adhesion and antibacterial properties. The obtained coatings were characterized by scanning electron microscopy, X-ray diffraction, and X-ray photoelectron spectroscopy, while their adhesion was measured using a scratch test. The maximum adhesion between the TiO₂ layer and the substrate was 39.8 ± 2.6 N at an anodizing voltage of 180 V. Subsequently, the CuHA coatings were successfully deposited on the TiO₂ layers and grown outward along TiO₂ pores (during this process, Cu atoms are doped into the HA structure in the form of Cu²⁺ ions). The CuHA adhesion to the TiO₂ layer was 26.3 ± 1.9 N, indicating that the TiO₂ interlayer significantly enhanced the bonding of CuHA to the substrate. Furthermore, the fabricated CuHA/TiO₂ coatings produced a strong antibacterial effect on *Escherichia coli* and *Staphylococcus aureus* species, exhibited high biocompatibility, and promoted the proliferation of MC3T3-E1 cells.

Keywords: TiO₂ nanopore, electrochemical deposition, Cu-doped hydroxyapatite coating, adhesion, antibacterial properties

1. Introduction

Ti and its alloys are widely used in biomedical implants, such as bone nails and artificial joints, because of their low density, excellent mechanical properties, and high biocompatibility (Ref 1, 2, 3, 4). However, Ti and its alloys are also biologically inert materials that, on account of their lack of biological activity, cannot promote the growth of bone tissues (Ref 5) and do not exhibit antibacterial properties, although bacterial infection and inflammation may occur after the long-term implantation of Ti-based materials into the human body (Ref 6). Therefore, the implant surface must be appropriately modified to enhance its osteogenic activity, adhesion, and antibacterial characteristics.

Hydroxyapatite (HA) is a main inorganic component of human bones that induces the growth of new bones (Ref 7, 8). However, HA does not possess antibacterial properties, and its adhesion to Ti substrates is relatively weak (Ref 9, 10), which limits its clinical applications (Ref 11, 12). Good adhesion between an HA coating and a Ti substrate is important but is often ignored in clinical practice. Electrochemical deposition (ED) is an effective method for preparing HA coatings due to the easy control over the coating composition, low fabrication cost, high processing speed, and high coating purity (Ref 13). However, because this method covers the substrate surface with a different material, the adhesion between the two components is relatively small. Say et al. (Ref 14) have found that the addition of SiO_2 to coatings produces a porous and crack-free surface morphology, which increases adhesion and corrosion resistance while reducing the pore density. Yigit et al. (Ref 15, 16) have prepared nano-hydroxyapatite-matrix coatings doped with different fractions of graphene nanosheets (GNS) on Ti-6Al-7Nb and Ti-6Al-4V alloy surfaces by plasma electrolytic oxidation and a hydrothermal method. They found that both the coating porosity and HA crystallinity increased with an increase in the GNS content. TiO_2 has attracted widespread attention owing to its high

corrosion resistance and ability to increase the bonding force between HA and the substrate (Ref 17, 18). In particular, TiO₂ nanopores can considerably improve the adhesion properties of the substrate and provide a suitable environment for cell growth (Ref 19, 20, 21). Dikici et al. (Ref 22) investigated the effects of rutile TiO₂ on a biphasic calcium phosphate (BCP) coating deposited on a β -type titanium alloy surface by a sol-gel method. They observed that this coating increased the scratch and corrosion resistances of the alloy. Anodic oxidization (AO) is a traditional surface modification method that can modify the chemical properties and structure of anodic films by varying parameters such as applied voltage, electrolyte composition and concentration, and temperature (Ref 23, 24). Therefore, it has become an attractive method for depositing oxide films on pure Ti surfaces. Multiple studies have revealed that an anatase or rutile TiO₂ film prepared by AO promoted apatite formation in a simulated body fluid (Ref 25, 26, 27). Recently, some metallic ions have been added to HA coatings to improve their antibacterial properties. A Zn-doped HA coating prepared by sol-gel and dip-coating methods was noncytotoxic. It produced strong antibacterial effects on *Escherichia coli* (*E. coli*) and *Staphylococcus aureus* (*S. aureus*), but its antibacterial activity was very limited (Ref 28). Ag-doped calcium TiO₂ coatings prepared by the thermochemical treatment of Ti surfaces demonstrated high antibacterial activity (Ref 29). However, Ag is an expensive metal that exhibits some cytotoxicity: Ag atoms may diffuse into cells through the “Trojan horse” mechanism and then release Ag⁺ ions that negatively affect intracellular functions (Ref 30, 31). In contrast, Cu is an inexpensive metal with excellent antibacterial ability. It is an essential trace element for maintaining the function of mammalian cells and produces anabolic effects on bone metabolism (Ref 32, 33, 34, 35). Furthermore, the continuous release of trace amounts of Cu²⁺ ions can induce the formation of new bones (Ref 36).

In a previous study, Cu-doped coatings with good antibacterial properties were prepared on Ti surfaces by ED (Ref 37). In the present study, to increase the adhesion between the coating and the substrate, an intermediate nanoporous TiO_2 layer was first deposited by AO, after which Cu-doped HA (CuHA) coatings were produced by ED. Finally, the surface properties, adhesion, antibacterial properties, and cytotoxicity of the fabricated composite coatings were determined by various techniques.

2. Experimental section

2.1. Sample preparation

Prior to electrochemical treatment, commercially pure Ti sheets (CP-Ti, purity: 99.5%) with sizes of $10 \times 10 \times 1 \text{ mm}^3$ were polished using 120–1200# SiC sandpaper and then ultrasonically cleaned with acetone, absolute ethanol, and distilled water for 15 min each. Subsequently, the Ti sheets were etched in a mixture of hydrofluoric and nitric acids with an $\text{HF}:\text{HNO}_3:\text{H}_2\text{O}$ volume ratio of 1:3:10 for 30 s. Finally, the sheets were ultrasonically cleaned in deionized water for 15 min and dried in a vacuum drying oven at 60°C .

To prepare a TiO_2 layer, two-electrode AO was carried out using direct current (Beijing Han Sheng Pu Yuan Technology Co., Ltd., HSPY-200-02) at constant voltages of 120, 150, and 180 V. This was performed in a water bath at a temperature of 25°C for 1 min using a Ti sheet as the anode, a platinum plate as the cathode, and a 2 mol/L H_2SO_4 solution as the electrolyte. The distance between cathodes and anodes was 2 cm. The obtained samples were termed as TiO_2 –120V, TiO_2 –150V, and TiO_2 –180V, respectively.

After the AO process, a Cu-containing HA coating was deposited by ED in a water bath set at 45

°C using a platinum sheet as the anode and the anodized sample as the cathode. The electrolyte consisted of 0.040 mol/L $\text{CaCl}_2 \cdot 2\text{H}_2\text{O}$, 0.025 mol/L $\text{NH}_4\text{H}_2\text{PO}_4$, and 0.001 mol/L $\text{CuCl}_2 \cdot 2\text{H}_2\text{O}$. Additionally, 0.1 mol/L NaCl was added to increase the solution conductivity. Samples were prepared at a constant voltage of 3 V for 7.5 and 15 min, after which they were ultrasonically cleaned with deionized water and dried in an oven at 60 °C. For convenience, the sample deposited for 7.5 min was termed as CuHA/TiO₂–7.5min, and the sample deposited for 15 min was labeled as CuHA/TiO₂–15min. For comparison, CuHA coatings without TiO₂ were deposited on CP-Ti at a voltage of 3 V and deposition times of 7.5 min and 15 min, which were termed as CuHA–7.5min and CuHA–15min, respectively.

2.2. Characterization techniques

Phase compositions and crystallinity were determined by X-ray diffraction (XRD, Bruker D8 Advance) with Cu K α radiation at a tube voltage of 40 kV, tube current of 40 mA, and scanning angles (2 θ) of 20°–80°. Surface morphologies were observed by scanning electron microscopy (SEM, FEI Quanta 450) at an accelerating voltage of 30 kV. Chemical compositions and elemental contents were analyzed by X-ray photoelectron spectroscopy (XPS, AIXS Ultra DLD) using a monochromatic Al K α ($h\nu = 1486.6$ eV) radiation source.

2.3. Adhesion test

The adhesion between the coating and the substrate was evaluated using an automatic scratch tester (Lanzhou Zhongke Kaihua Technology Development Co., Ltd., WS-2005), which contained a diamond indenter with a tip radius of 0.2 mm. Measurements were performed at an antenna angle of

120°, a load of 50 N, a load rate of 30 N/min, and a scratch length of 3 mm. Each sample was tested three times.

2.4. Evaluation of antibacterial properties

The antibacterial properties of the fabricated coatings were evaluated using *S. aureus* ATCC 29213 and *E. coli* ATCC 25922 cells. The number of colonies was measured by a plate counting method. TiO₂-180V, CuHA/TiO₂-7.5min, and CuHA/TiO₂-15min were subjected to antibacterial tests using CP-Ti as the control group. After sterilization in a high-temperature, high-pressure steam sterilizer for 20 min, the samples were added to a 24-well plate. The bacterial solution was diluted to 10⁶ CFU/mL with Luria–Bertani (LB) liquid medium, and 0.2 mL of the diluted bacterial solution was added to the surface of a studied sample. Sterile normal saline was added to the empty wells to prevent water evaporation from the bacterial solution. The 24-well plate was placed in a constant-temperature incubator at 37 °C for 18 h. After the co-cultivation was complete, the co-culture solution was diluted to 10⁶ CFU/mL with a sterile phosphate-buffered saline (PBS) solution. Afterward, 100 µL of each diluted solution was evenly applied to the LB solid medium, which was then placed in a constant-temperature incubator at 37 °C for 18 h for static culture. At the end of this process, the number of colonies was recorded. The antibacterial rate was calculated via the following formula: antibacterial rate (%) = (CFU of the control sample – CFU of the tested sample) / CFU of the control sample × 100%.

2.5. Cytotoxicity test

MC3T3-E1 cells (iCell Bioscience Inc.) were used to evaluate the cytotoxicity of the produced

coatings. The culture medium was α -MEM (Corning Inc.) supplemented with 10% fetal bovine serum (Biological Industries). CP-Ti, CuHA/TiO₂-7.5min, and CuHA/TiO₂-15min were selected for the cytocompatibility studies. The samples were first sterilized at high temperature and pressure. As the samples contained solid flakes, extraction was conducted at 37 °C for 24 h at a surface area/liquid volume ratio of 1.25 cm²/mL following the ISO10993-12 standard. Each sample extract (100 μ L) was placed into separate 96-well plates, and three parallel wells were set up for each sample. The MC3T3-E1 cells were inoculated into each well at densities of 2×10^3 cells/well for 1-d culturing and 1×10^3 cells/mL for 4-d and 7-d culturing. The 96-well plates were placed in a humidified incubator with a 5% CO₂ atmosphere for 1, 4, and 7 d at 37 °C. After culturing, each well was rinsed three times with PBS. The culture medium (100 μ L) with 10% MTT assay was added to each well and then incubated in a humidified incubator with a 5% CO₂ atmosphere for an additional 4 h at 37 °C. The supernatant was aspirated, and 100 μ L of dimethyl sulfoxide was added to each well, followed by gentle shaking for 10 min. Optical density (OD) was measured at a wavelength of 570 nm using a TECAN SPARK 10M enzyme-labeled instrument. As a control, MC3T3-E1 cells were directly seeded onto the bottoms of the wells without extracts.

3. Results and discussion

3.1. Adhesion properties of TiO₂ nanopores

SEM images of the TiO₂ nanopores prepared at 120, 150, and 180 V are shown in Fig. 1. During the AO process, gas evolution and spark discharge occurred. After AO, a TiO₂ layer with a three-dimensional oxidation structure composed of numerous open pores was formed on the CP-Ti surface. Uniformly distributed nanopores with average sizes of approximately 100 nm were produced on the

TiO₂-120V surface (Fig. 1a). The pores increased in size and became non-uniform as the voltage increased from 120 to 150 V (Fig. 1b). For TiO₂-180V, an alternating sequence of large and small holes was observed (Fig. 1c). The obtained XRD patterns (Fig. 2) showed that the TiO₂-120V sample mainly consisted of Ti and anatase species, while TiO₂-150V contained Ti, anatase, and rutile components. The main phases of TiO₂-180V were Ti and rutile, and only a small peak corresponding to anatase was observed at 25.8°. It has been previously reported that a mixed structure of rutile and anatase TiO₂ exhibited high chemical stability and good mechanical properties (Ref 38). Yang et al. have demonstrated that TiO₂ with specific anatase and rutile structures could induce apatite formation in vitro (Ref 39). Additionally, rutile TiO₂ has been reported to promote apatite deposition because of lattice matching between the rutile and apatite phases (Ref 40).

The scratch method was used to determine the adhesion between the TiO₂ layer and the substrate. The friction and acoustic signal curves of the samples prepared at different voltages are shown in Fig. 3. A sudden increase in the acoustic signal accompanied by a significant change in the friction, which occurs when the coating is completely peeled off. The corresponding load is called a critical load. The adhesions of TiO₂-120V, TiO₂-150V, and TiO₂-180V were equal to 32.2 ± 2.1 , 34.7 ± 2.5 , and 39.8 ± 2.6 N, respectively. Thus, the adhesion of the TiO₂ layer increased with increasing voltage, which was likely due to the alternating sequence of large and small holes. Such a multilevel structure facilitates mechanical interlocking and enhances coating adhesion. As the TiO₂-180V sample mainly consisted of rutile and exhibited the highest adhesion, the Cu-containing HA coatings were subsequently prepared on its surface.

3.2. Coating structure

The SEM images of the composite coatings are displayed in Fig. 4. Specifically, Fig. 4a shows that the nanopores are completely covered by dense flocculent crystals. After increasing the deposition time from 7.5 to 15 min, the crystals continued to aggregate and cluster together, producing a “community” distribution on the coating surface (Fig. 4b). Fig. 5 reveals the XRD patterns of Cu-doped HA coatings. In the figure, the diffraction peaks of HA are observed at the 2θ values of 25.9° , 28.1° , 32.2° , and 35.4° (JCPDS No. 09-0432) (Ref 37, 41). The characteristic diffraction peaks of Ti are also observed in all samples. For CuHA/TiO₂–7.5min and CuHA/TiO₂–15min, the rutile TiO₂ peaks appeared. The crystallinity of Cu-doped HA coatings is listed in Table 1. The crystallinity of the CuHA–7.5min and CuHA–15min coatings was $81.26 \pm 4.67\%$ and $80.12 \pm 4.27\%$, respectively. The addition of titanium dioxide reduced the crystallinity of CuHA/TiO₂–7.5min and CuHA/TiO₂–15min to $67.01 \pm 3.59\%$ and $64.82 \pm 3.55\%$, respectively. This is because TiO₂ is a semiconductor with lower electrical conductivity than that of pure titanium, which hinders the electrochemical deposition process to a certain extent and inhibits the crystallization of HA.

The chemical compositions of the obtained samples measured by XPS are listed in Table 2. The Cu content in the coatings increased from 1.44 to 2.53% as deposition time increased from 7.5 to 15 min. The full XPS profiles (Figs. 6a and c) indicate that the coatings mainly consisted of the elements Ca, P, Cu, O, C, and N. The observed C peak is likely caused by the dissolved carbon dioxide in the electrolyte (Ref 33). The high-resolution Cu spectra (Figs. 6b and d) contain peaks with binding energies of 934.2 and 936.8 eV, corresponding to Cu–OH and Cu–PO₄ bonds, respectively (Ref 37, 42), as well as Cu²⁺ satellite peaks suggesting the presence of Cu atoms in the HA structure in the form of Cu²⁺ ions, which react with OH[–] and PO₄^{3–} ions. Thus, it can be concluded that Cu atoms are doped into the HA lattice as Cu²⁺ ions.

3.3. Adhesion of composite coatings

The results of scratch testing demonstrated a relationship between the load, acoustic signal, and friction. Friction fluctuations are strongly related to the coating microstructure (Ref 43), which can be observed in Fig. 7. The coating starts peeling off at high loads, as indicated by the observed scratch morphology. As illustrated in Fig. 7a, the entire process, from the contact of the diamond indenter with the coating to the peeling of the coating, can be divided into three stages. In the first stage, the load is low; cracks begin to form inside the coating, and slight plastic deformation is observed on the coating surface. As a result, the scratches on the coating surface are relatively narrow; further, the surface friction is low, and the acoustic emission signal value is stable. During the second stage, the coating continues to plastically deform as the load further increases. After the diamond indenter scratches the coating, the rebound of the metal substrate produces transverse cracks on the coating surface, which extend in different directions. When the load reaches a certain value, the friction factor between the substrate and the coating changes. Simultaneously, the noise generated when the coating is peeled off causes a sudden change in the acoustic emission signal (the corresponding load is called a critical load). After the coating is peeled off, the diamond indenter directly touches the substrate, and the friction increases with increasing load. During the third stage, when the load is equal to approximately 33 N, the friction reaches a maximum and then remains constant.

As seen in Figs. 7a–c, the friction of the CuHA/TiO₂–7.5min composite coating was observed to suddenly decrease along with a rapid change in the acoustic emission signal at a load of approximately 26 N because the coating completely peeled off. The adhesion of the CuHA/TiO₂–7.5min composite determined from the results of three different scratch tests was 26.3 ± 1.9 N. Similarly, the adhesion

of the CuHA coating was equal to 11.2 ± 1.4 N. Our findings compare favorably to those of Surmenev et al.; they prepared an HA coating by radio-frequency magnetron sputtering, which began to fall off at 5.5 N and was completely detached at a load of approximately 13.5 N (Ref 44). The adhesion of a coating prepared by radio-frequency magnetron sputtering is usually higher than that of a coating prepared via ED. However, in our work, the adhesion between HA and the substrate is relatively high owing to the presence of TiO_2 nanopores in the CuHA/ TiO_2 composite coating. Possible reasons for this phenomenon can be summarized as follows. (a) The Ti oxide particles present on the surface of the TiO_2 porous layer increase the coating roughness and adhesion (Ref 45). (b) The OH^- ions on the surface of TiO_2 nanopores react to produce $\text{Ti}(\text{OH})_2 \cdot \text{H}_2\text{O}$ species, which form chemical bonds with the CuHA coating. The obtained Ti– TiO_2 –HA structure strengthens the bonds between the coating and the substrate (Ref 46). (c) The thermodynamic expansion coefficients of the CP-Ti and CuHA coatings are equal to 10.8×10^{-6} /K and 15×10^{-6} /K, respectively. Their difference generates residual thermal stress and instantaneous thermal stress. The thermodynamic expansion coefficient of TiO_2 is 10.2×10^{-6} /K, which is close to that of CP-Ti. Thus, the residual stress generated by the mismatch between the thermodynamic expansion coefficients of the CuHA coating and CP-Ti substrate is buffered, inhibiting the formation of microcracks and effectively reducing the coating shedding probability (Ref 9, 47,48). (d) The CuHA coating begins to grow on the nanopore and forms a compact CuHA/ TiO_2 layer with improved adhesion properties (Ref 45).

3.4. Antibacterial properties

Figure 8 depicts the colonies of *E. coli* and *S. aureus* after culturing at 37 °C for 24 h. For CP-Ti, numerous colonies are observed on the agar plate, which is consistent with the poor antibacterial

property of Ti and its alloys (Ref 49). For TiO₂-180V, the number of colonies is slightly reduced due to the limited antibacterial properties of this sample (its antibacterial rates for *E. coli* and *S. aureus* are only 26.8% and 23.1%, respectively). For the CuHA/TiO₂ composite coatings, the number of colonies on the corresponding plates were sharply reduced. The antibacterial rates of CuHA/TiO₂-7.5min for *E. coli* and *S. aureus* were equal to 87% and 85%, respectively. Moreover, the antibacterial rates of CuHA/TiO₂-15min for the same cultures were 96.1% and 95.8%, respectively. Therefore, both CuHA/TiO₂ composite coatings exhibit strong antibacterial properties. Note that the antibacterial properties of all coatings against *S. aureus* were not as good as those against *E. coli* because the cell walls of *S. aureus* are thicker than the cell walls of *E. coli* (Ref 33,50). With an increase in the Cu content, the antibacterial rate increased significantly, which is consistent with the conclusions of Liu et al. (Ref 51). The results clearly demonstrated that the Cu-doped composite coatings possessed good antibacterial properties.

3.5. Cytotoxicity

The cytotoxicity of the CuHA/TiO₂ coatings was evaluated by conducting MTT tests using MC3T3-E1 as a cell model. As shown in Fig. 9, after 1 day of culture, the OD values of each group remained similar, and their differences were not statistically significant. After 4 d, the OD values of all samples increased, indicating that the cells proliferate with increasing culture time. The OD values of the CP-Ti and CuHA/TiO₂ coatings were significantly higher than that of the control group ($P < 0.01$). However, the difference between these two samples was not statistically significant. After 7 d of culture, the OD values of all groups further increased, and no statistically significant difference between CP-Ti and CuHA/TiO₂-7.5min was observed. The OD value of CuHA/TiO₂-15min was

1
2
3
4
5
6
7
8
9
10
11
12
13
14
15
16
17
18
19
20
21
22
23
24
25
26
27
28
29
30
31
32
33
34
35
36
37
38
39
40
41
42
43
44
45
46
47
48
49
50
51
52
53
54
55
56
57
58
59
60

much lower than those of CP-Ti and CuHA/TiO₂–7.5min, although it was significantly higher than the OD of the control group, suggesting that CuHA/TiO₂–15min exhibits good cytocompatibility. The results indicate that the Cu-doped HA/TiO₂ composite coatings demonstrate no cytotoxicity against osteoblast cells. However, excessive Cu amounts are known to increase their cytotoxicity considerably (Ref 52). In this study, the Cu content was maintained at a relatively low level by adjusting the deposition time. The fabricated composite coatings possessed enhanced adhesion and antibacterial properties without cytotoxicity; therefore, the proposed method is suitable for preparing antibacterial coatings.

4. Conclusion

In summary, novel antibacterial and biocompatible CuHA/TiO₂ composite coatings were prepared by AO combined with ED. The TiO₂ nanopores fabricated by AO at 180 V exhibited good adhesion properties and increased the adhesion of composite coatings when used as intermediate layers. During deposition, Cu atoms were doped into the HA structure in the form of Cu²⁺ ions. The Cu content increased from 1.44 to 2.53 at.% with an increase in deposition time from 7.5 to 15 min, while the Cu doping of HA significantly enhanced its antibacterial properties without exhibiting cytotoxicity. Thus, the proposed two-step ED method can be used to improve the adhesion and antibacterial properties of coated implants.

Acknowledgements

This work was partially supported by the Natural Science Foundation of Shanghai, China (No. 15ZR1428400), Shanghai Engineering Research Center of High-Performance Medical Device

Materials (No. 20DZ2255500), and the Grant-in Aid for Scientific Research (C) (No. 20K05139) from JSPS (Japan Society for the Promotion of Science), Tokyo, Japan.

For Peer Review

References

1. J. Wang, Y.A. Qing, L.G. Xiao, Y.G. Wang, X.F. Bao, Y.G. Qin, J.Y. Zhang, K. Zhang, Design of new-type F-FLC artificial joint coatings via fluorine incorporation and fullerene-like structure construction, *Surf. Coat. Tech.*, 2020, 385, p 125419, in English.
2. M. Pettersson, T. Berlind, S. Schmidt, S. Jacobson, L. Hultman, C. Persson, H. Engqvist, Structure and composition of silicon nitride and silicon carbon nitride coatings for joint replacements. *Surf. Coat. Tech.*, 2013, 235, p 827-834, in English.
3. M. Cuervas-Mons, E. León-Román, C. Solans, Á. Martínez-Ayora, J. Vaquero, Retrograde tibial nail and trabecular titanium spacer block for the treatment of missing talus: A Rare case report. *J. Foot Ankle Surg.*, 2020, 59(1), p 184-189, in English.
4. L. Korhonen, M. Perhomaa, A. Kyrö, T. Pokka, W. Serlo, J. Merikanto, J.-J. Sinikumpu, Intramedullary nailing of forearm shaft fractures by biodegradable compared with titanium nails: Results of a prospective randomized trial in children with at least two years of follow-up. *Biomaterials*, 2018, 185, p 383-392, in English.
5. A. Civantos, E. Martínez-Campos, V. Ramos, C. Elvira, A. Gallardo, A. Abarrategi, Titanium coatings and surface modifications: toward clinically useful bioactive implants. *ACS Biomater. Sci. Eng.*, 2017, 3(7), p 1245-1261, in English.
6. N.A. Hodges, E.M. Sussman, J.P. Stegemann, Aseptic and septic prosthetic joint loosening: Impact of biomaterial wear on immune cell function, inflammation, and infection. *Biomaterials*, 2021, 278, p 121127, in English.
7. L. Fathyunes, J. Khalil-Allafi, S.O.R. Sheykholeslami, M. Moosavifar, Biocompatibility assessment of graphene oxide-hydroxyapatite coating applied on TiO₂ nanotubes by ultrasound-assisted pulse electrodeposition. *Mat. Sci. Eng. C-Mater.*, 2018, 87, p 10-21, in English.

8. N. Karimi, M. Kharaziha, K. Raeissi, Electrophoretic deposition of chitosan reinforced graphene oxide-hydroxyapatite on the anodized titanium to improve biological and electrochemical characteristics. *Mat. Sci. Eng. C-Mater.*, 2019, 98, p 140-152, in English.
9. D.L. Qiu, L.J. Yang, Y.S. Yin, A.P. Wang, Preparation and characterization of hydroxyapatite/titania composite coating on NiTi alloy by electrochemical deposition. *Surf. Coat. Tech.*, 2011, 205(10), p 3280-3284, in English.
10. Z.J. Wu, L.P. He, Z.Z. Chen, Composite biocoating of hydroxyapatite/ Al_2O_3 on titanium formed by Al anodization and electrodeposition. *Mater. Lett.*, 2007, 61(14-15), p 2952-2955, in English.
11. L. Suo, N. Jiang, Y. Wang, P.Y. Wang, J.Y. Chen, X.B. Pei, J. Wang, Q.B. Wan, The enhancement of osseointegration using a graphene oxide/chitosan/hydroxyapatite composite coating on titanium fabricated by electrophoretic deposition. *J. Biomed. Mater. Res. B*, 2019, 107, p 635-645, in English.
12. Y.H. Duan, S. Zhu, F. Gao, J.Y. Zhu, M. Li, J. Ma, Q.S. Zhu, The effect of adhesive strength of hydroxyapatite coating on the stability of hydroxyapatite-coated prostheses in vivo at the early stage of implantation. *Arch. Med. Sci.*, 2012, 8, p 199-208, in English.
13. M. Hadidi, A. Bigham, E. Saebnoori, S.A. Hassanzadeh-Tabrizi, S. Rahmati, Z.M. Alizadeh, V. Nasirian, M. Rafienia, Electrophoretic-deposited hydroxyapatite-copper nanocomposite as an antibacterial coating for biomedical applications. *Surf. Coat. Tech.*, 2017, 321, p 171-179, in English.
14. Y. Say, B. Aksakal, B. Dikici, Effect of hydroxyapatite/ SiO_2 hybride coatings on surface morphology and corrosion resistance of REX-734 alloy. *Ceram. Int.*, 2016, 42(8), p 10151-10158, in English.
15. O. Yigit; N. Ozdemir, B. Dikici, M. Kaseem, Surface Properties of Graphene Functionalized

- TiO₂/nHA Hybrid Coatings Made on Ti6Al7Nb Alloys via Plasma Electrolytic Oxidation (PEO). *Molecules*, 2021, 26(13), p 3903, in English.
16. O. Yigit, B. Dikici, T.C. Senocak, N. Ozdemir, One-step synthesis of nano-hydroxyapatite/graphene nanosheet hybrid coatings on Ti6Al4V alloys by hydrothermal method and their in-vitro corrosion responses. *Surf. Coat. Tech.*, 2020, 394, p 125858, in English.
17. Y. Wu, Q.Q. Li, B.Y. Xu, H.Y. Fu, Y. Li, Nano-hydroxyapatite coated TiO₂ nanotubes on Ti-19Zr-10Nb-1Fe alloy promotes osteogenesis in vitro. *Colloids Surf. B*, 2021, 207, p 112019, in English.
18. X.J. Long, L. Duan, W.J. Weng, K. Cheng, D.P. Wang, H.W. Ouyang, Light-induced osteogenic differentiation of BMSCs with graphene/TiO₂ composite coating on Ti implant. *Colloids Surf. B*, 2021, 207, p 111996, in English.
19. X. Cui, H.-M. Kim, M. Kawashita, L. Wang, T. Xiong, T. Kokubo, T. Nakamura, Preparation of bioactive titania films on titanium metal via anodic oxidation. *Dent. Mater.*, 2009, 25(1), p 80-86, in English.
20. S. Khanmohammadi, M. Ojaghi-Ilkhchi, M. Farrokhi-Rad, Development of bioglass coating reinforced with hydroxyapatite whiskers on TiO₂ nanotubes via electrophoretic deposition. *Ceram. Int.*, 2021, 47(1), p 1333-1343, in English.
21. B. Feng, X.J. Chu, J.M. Chen, J.X. Wang, X. Lu, J. Weng, Hydroxyapatite coating on titanium surface with titania nanotube layer and its bond strength to substrate. *J. Porous Mater.*, 2010, 17(4), p 453-458, in English.
22. B. Dikici, M. Niinomi, M. Topuz, S.G. Koc, M. Nakai, Synthesis of biphasic calcium phosphate (BCP) coatings on β -type titanium alloys reinforced with rutile-TiO₂ compounds: adhesion resistance

and in-vitro corrosion. *J. Sol-Gel Sci. Technol.* 2018, 87, p 713–724, in English.

23 Y.-T. Sul, C.B. Johansson, S. Petronis, A. Krozer, Y. Jeong, A. Wennerberg, T. Albrektsson, Characteristics of the surface oxides on turned and electrochemically oxidized pure titanium implants up to dielectric breakdown: the oxide thickness, micropore configurations, surface roughness, crystal structure and chemical composition. *Biomaterials*, 2002, 23(2), p 491-501, in English.

24. Y.-T. Sul, C.B. Johansson, Y. Jeong, T. Albrektsson, The electrochemical oxide growth behaviour on titanium in acid and alkaline electrolytes. *Med. Eng. Phys.*, 2001, 23(5), p 329-346, in English.

25. X.I. Zhu, K.-H. Kim, Y. Jeong, Anodic oxide films containing Ca and P of titanium biomaterial. *Biomaterials*, 2001, 22(16), p 2199-2206, in English.

26. D. Velten, V. Biehl, F. Aubertin, B. Valeske, W. Possart, J. Breme, Preparation of TiO₂ layers on cp-Ti and Ti6Al4V by thermal and anodic oxidation and by sol-gel coating techniques and their characterization. *J. Biomed. Mater. Res.*, 2002, 59(1), p 18-28, in English.

27. R. Rohanizadeh, M. Al-Sadeq, R.Z. Legeros, Preparation of different forms of titanium oxide on titanium surface: effects on apatite deposition. *J. Biomed. Mater. Res. A*, 2004, 71(2), p 343-352. in English.

28. Q. Bi, X. Song, Y.J. Chen, Y.P. Zheng, P. Yin, T. Lei, Zn-HA/Bi-HA biphasic coatings on Titanium: Fabrication, characterization, antibacterial and biological activity. *Colloids Surf. B*, 2020, 189, p 110813, in English.

29. A. Rodríguez-Contreras, D. Torres, B. Rafik, M. Ortiz-Hernandez, M.P. Ginebra, J.A. Calero, J.M. Manero, E. Ruperez, Bioactivity and antibacterial properties of calcium- and silver-doped coatings on 3D printed titanium scaffolds. *Surf. Coat. Tech.*, 2021, 421, p 127476, in English.

30. H. Hu, W. Zhang, Y. Qiao, X. Jiang, X. Liu, C. Ding, Antibacterial activity and increased bone

- marrow stem cell functions of Zn-incorporated TiO₂ coatings on titanium. *Acta Biomater.*, 2012, 8(2), p 904-915, in English.
31. E.-J. Park, J. Yi, Y. Kim, K. Choi, K. Park, Silver nanoparticles induce cytotoxicity by a Trojan-horse type mechanism. *Toxicol. In Vitro*, 2010, 24(3), p 872-878, in English.
32. M. Thukkaram, M. Vaidulych, O. Kylián, P. Rigole, S. Aliakbarshirazi, M. Asadian, A. Nikiforov, H. Biederman, T. Coenye, G.D. Laing, R. Morent, A.V. Tongel, L.D. Wilde, K. Verbeken, N.D. Geyter, Biological activity and antimicrobial property of Cu/a-C:H nanocomposites and nanolayered coatings on titanium substrates. *Mat. Sci. Eng. C-Mater.*, 2021, 119, p 111513, in English.
33. H.B. Wu, X.Y. Zhang, Z.H. Geng, Y. Yin, R.Q. Hang, X.B. Huang, X.H. Yao, B. Tang, Preparation, antibacterial effects and corrosion resistant of porous Cu–TiO₂ coatings. *Appl. Surf. Sci.*, 2014, 308, p 43-49, in English.
34. A. Hoppe, N.S. Güldal, A.R. Boccaccini, A review of the biological response to ionic dissolution products from bioactive glasses and glass-ceramics. *Biomaterials*, 2011, 32(11), p 2757-2774, in English.
35. I. Burghardt, F. Lüthen, C. Prinz, B. Kreikemeyer, C. Zietz, H.-G. Neumann, J. Rychly, A dual function of copper in designing regenerative implants. *Biomaterials*, 2015, 44, p 36-44, in English.
36. N.J. Lakhkar, I.-H. Lee, H.-W. Kim, V. Salih, I.B. Wall, J.C. Knowles, Bone formation controlled by biologically relevant inorganic ions: Role and controlled delivery from phosphate-based glasses. *Adv. Drug. Delivery Rev.*, 2013, 65(4), p 405-420, in English.
37. Q. Li, J.S. Yang, J.J. Li, R. Zhang, M. Nakai, M. Niinomi, T. Nakano, Antibacterial Cu-doped calcium phosphate coating on pure titanium. *Mater. Trans.*, 2021, 62(7), p 1052-1055, in English.
38. F. Hilario, V. Roche, R.P. Nogueira, A.M.J. Junior, Influence of morphology and crystalline

- structure of TiO₂ nanotubes on their electrochemical properties and apatite-forming ability. *Electrochim. Acta*, 2017, 245, p 337-349, in English.
39. B.C. Yang, M. Uchida, H.-M. Kim, X.D. Zhang, T. Kokubo, Preparation of bioactive titanium metal via anodic oxidation treatment. *Biomaterials*, 2004, 25(6), p 1003-1010, in English.
40. S. Ban, S. Maruno, A. Harada, M. Hattori, K. Narita, J. Hasegawa, Effect of temperature on morphology of electrochemically-deposited calcium phosphates. *Dent. Mater. J.*, 1996, 15(1), p 31-38, in English.
41. L. Ling, T.T. Li, M.C. Lin, Q. Jiang, H.T. Ren, C.W. Lou, J.H. Lin, Effect of hydrogen peroxide concentration on the nanostructure of hydroxyapatite coatings via ultrasonic-assisted electrodeposition. *Mater. Lett.*, 2020, 261, p 126989, in English.
42. M.C. Biesinger, Advanced analysis of copper X-ray photoelectron spectra. *Surf. Interface Anal.*, 2017, 49(13), p 1325-1334, in English.
43. H. Pelletier, A. Carrado, J. Faerber, I.N. Mihailescu, Microstructure and mechanical characteristics of hydroxyapatite coatings on Ti/TiN/Si substrates synthesized by pulsed laser deposition. *Appl. Phys. A*, 2011, 102(3), p 629-640, in English.
44. R.A. Surmenev, I.Y. Grubova, E. Neyts, A.D. Teresov, N.N. Koval, M. Epple, A.I. Tyurin, V.F. Pichugin, M.V. Chaikina, M.A. Surmeneva, Ab initio calculations and a scratch test study of RF-magnetron sputter deposited hydroxyapatite and silicon-containing hydroxyapatite coatings. *Surf. Interfaces*, 2020, 21, p 100727, in English.
45. S. Ahmadi, I. Mohammadi, S.K. Sadrnezhad, Hydroxyapatite based and anodic Titania nanotube biocomposite coatings: Fabrication, characterization and electrochemical behavior. *Surf. Coat. Tech.*, 2016, 287, p 67-15, in English.

46. C.-M. Lin, S.-K. Yen, Characterization and bond strength of electrolytic HA/TiO₂ double layers for orthopedic applications. *J. Mater. Sci.-Mater. M.*, 2004, 15(11), p 1237-1246, in English.
47. H. Farnoush, J.A. Mohandesi, H. Çimenoglu, Micro-scratch and corrosion behavior of functionally graded HA-TiO₂ nanostructured composite coatings fabricated by electrophoretic deposition. *J. Mech. Behav. Biomed.*, 2015, 46, p 31-40, in English.
48. W.J. Weng, S. Zhang, K. Cheng, H.B. Qu, P.Y. Du, G. Shen, J. Yuan, G.R. Han, Sol-gel preparation of bioactive apatite films. *Surf. Coat. Tech.*, 2003, 167(2-3), p 292-296, in English.
49. S.L. Mei, H.Y. Wang, W. Wang, L.P. Tong, H.B. Pan, C.S. Ruan, Q.L. Ma, M.Y. Liu, H.L. Yang, L. Zhang, Y.C. Cheng, Y.M. Zhang, L.Z. Zhao, P.K. Chu, Antibacterial effects and biocompatibility of titanium surfaces with graded silver incorporation in titania nanotubes. *Biomaterials*, 2014, 35(14), p 4255-4265, in English.
50. N. Murugan, C. Murugan, A.K. Sundramoorthy, In vitro and in vivo characterization of mineralized hydroxyapatite/polycaprolactone-graphene oxide based bioactive multifunctional coating on Ti alloy for bone implant applications. *Arabian J. Chem.*, 2018, 11(6), p 959-969, in English.
51. J. Liu, F.B. Li, C. Liu, H.Y. Wang, B.R. Ren, K. Yang, E.L. Zhang, Effect of Cu content on the antibacterial activity of titanium-copper sintered alloys. *Mat. Sci. Eng. C-Mater.*, 2014, 35(1), p 392-400, in English.
52. R.Q. Hang, A. Gao, X.B. Huang, X.G. Wang, X.Y. Zhang, L. Qin, B. Tang, Antibacterial activity and cytocompatibility of Cu-Ti-O nanotubes. *J. Biomed. Mater. Res. A*, 2014, 102(6), p 1850-1858, in English.

Table 1. Crystallinity of Cu-doped HA coatings.

Sample	CuHA–7.5min	CuHA–15min	CuHA/TiO ₂ –7.5min	CuHA/TiO ₂ –15min
Crystallinity	81.26 ± 4.67%	80.12 ± 4.27%	67.01 ± 3.59%	64.82 ± 3.55%

Table 2. Chemical compositions (at.%) of the samples measured by XPS.

Sample	Ti	O	Cu	P	Ca
CuHA/TiO ₂ –7.5min	0.02 ± 0.17	66.25 ± 0.46	1.44 ± 0.27	15.05 ± 0.39	17.33 ± 0.26
CuHA/TiO ₂ –15min	0.01 ± 0.10	66.19 ± 0.43	2.53 ± 0.27	15.11 ± 0.33	16.16 ± 0.25

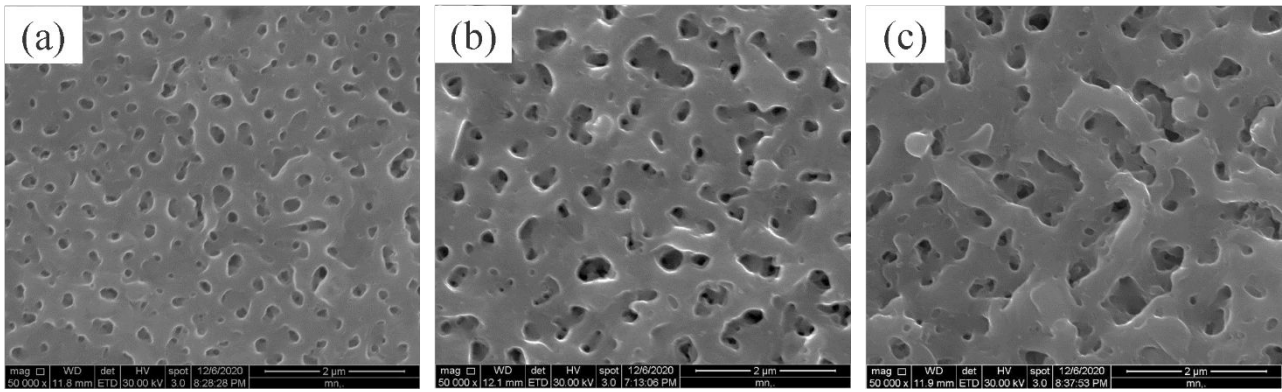


Fig. 1. SEM images of (a) TiO₂-120V, (b) TiO₂-150V, and (c) TiO₂-180V.

For Peer Review

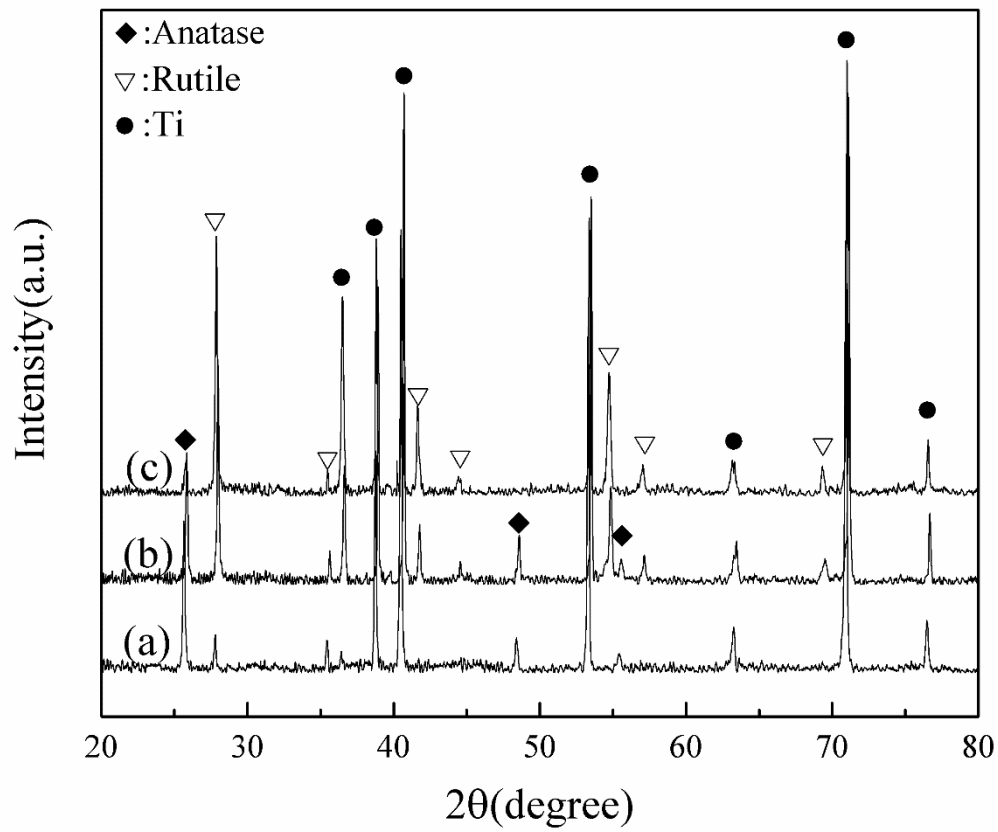


Fig. 2. XRD patterns of (a) TiO_2 -120V, (b) TiO_2 -150V, and (c) TiO_2 -180V.

1
2
3
4
5
6
7
8
9
10
11
12
13
14
15
16
17
18
19
20
21
22
23
24
25
26
27
28
29
30
31
32
33
34
35
36
37
38
39
40
41
42
43
44
45
46
47
48
49
50
51
52
53
54
55
56
57
58
59
60

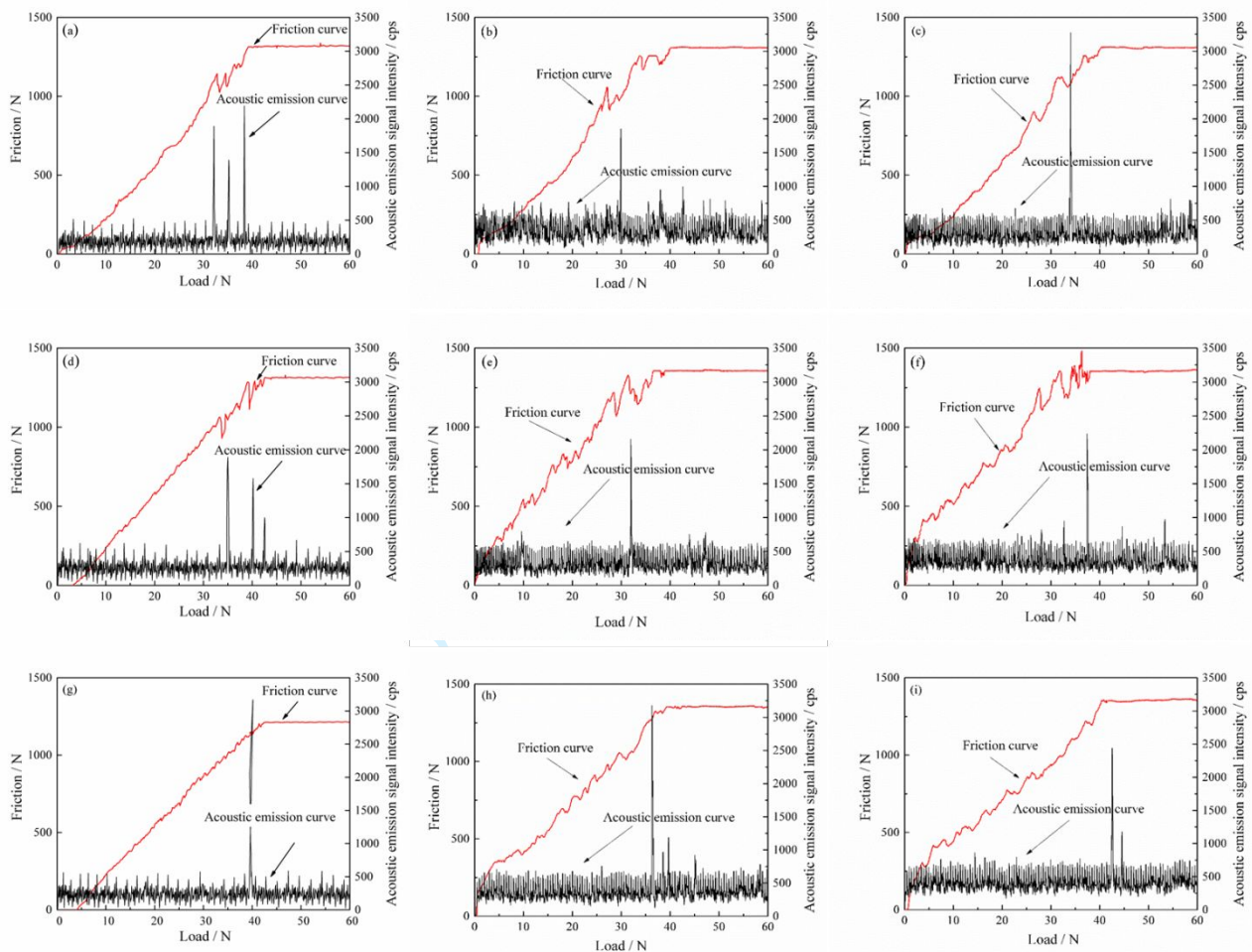


Fig. 3. Friction and acoustic signal curves of (a)–(c) TiO_2 –120V, (d)–(f) TiO_2 –150V, and (g)–(i) TiO_2 –180V.

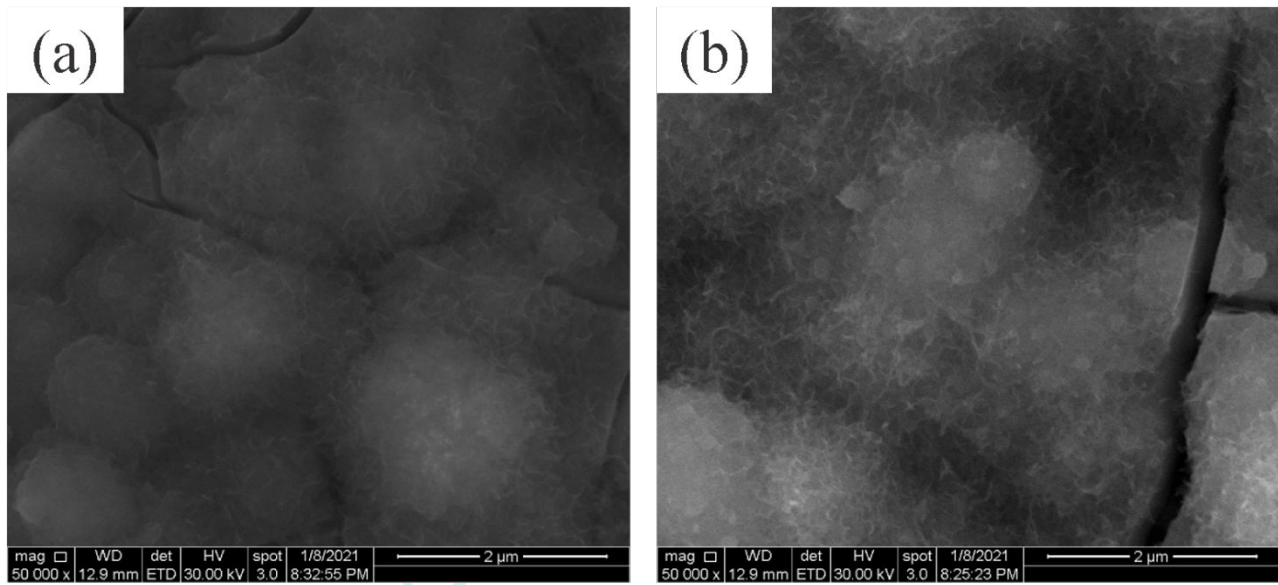


Fig. 4. SEM images of (a) CuHA/TiO₂–7.5min and (b) CuHA/TiO₂–15min.

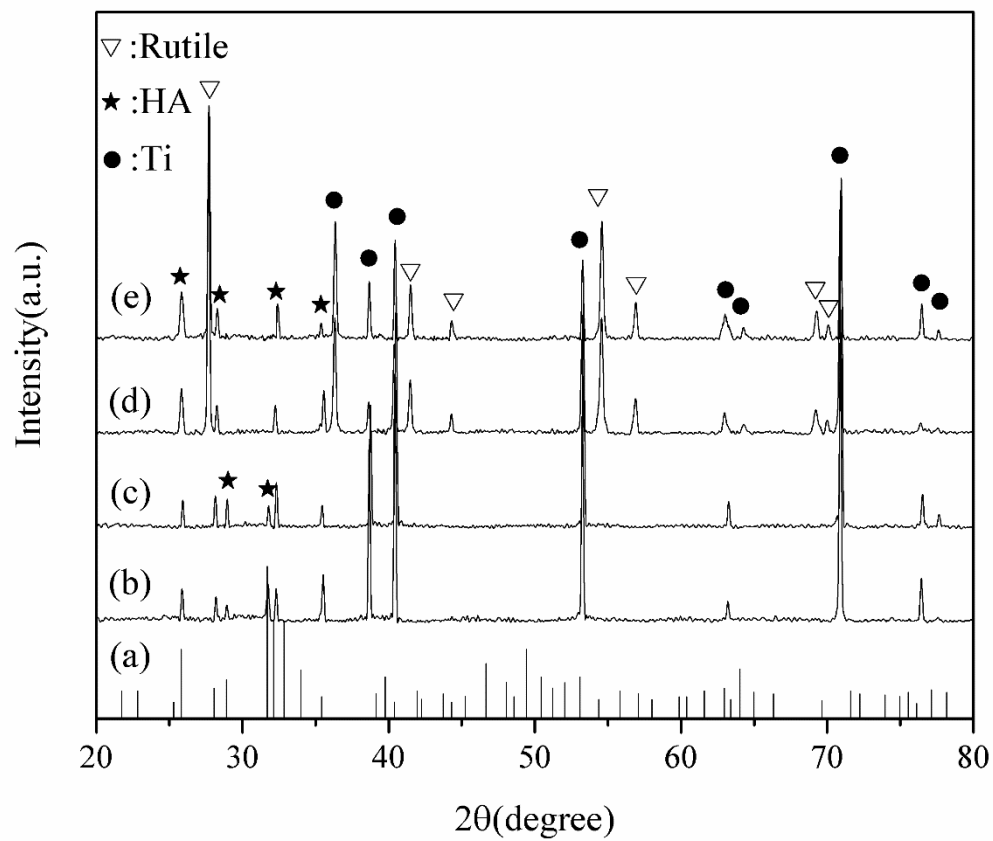


Fig. 5. (a) HA pattern ICCD 09-0432 and XRD patterns of (b) CuHA–7.5min, (c) CuHA–15min, (d) CuHA/TiO₂–7.5min, and (e) CuHA/TiO₂–15min.

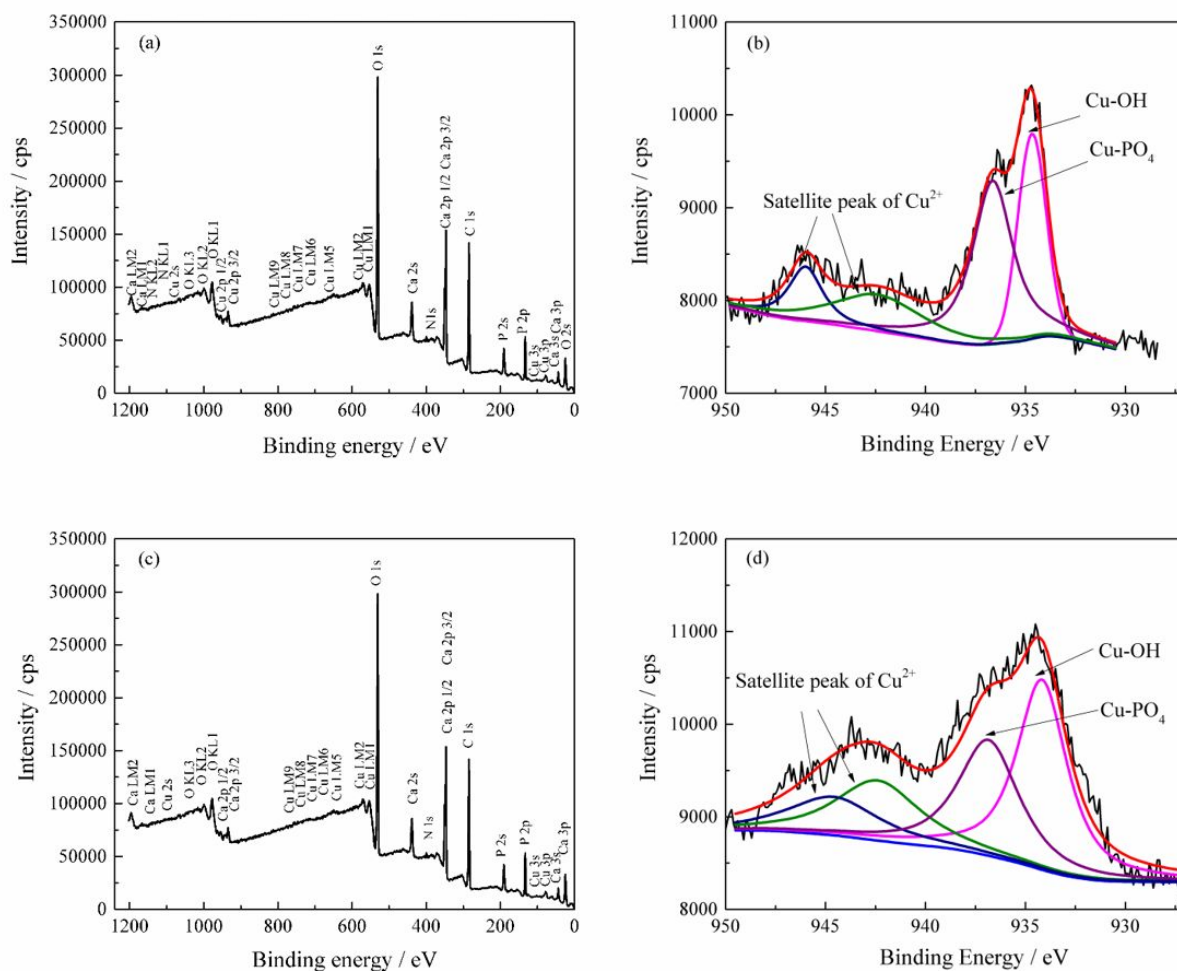


Fig. 6. XPS survey spectra (a, c) and Cu 2p high-resolution spectra (b, d) of (a) (b) CuHA/TiO₂-7.5min and (c) (d) CuHA/TiO₂-15min.

1
2
3
4
5
6
7
8
9
10
11
12
13
14
15
16
17
18
19
20
21
22
23
24
25
26
27
28
29
30
31
32
33
34
35
36
37
38
39
40
41
42
43
44
45
46
47
48
49
50
51
52
53
54
55
56
57
58
59
60

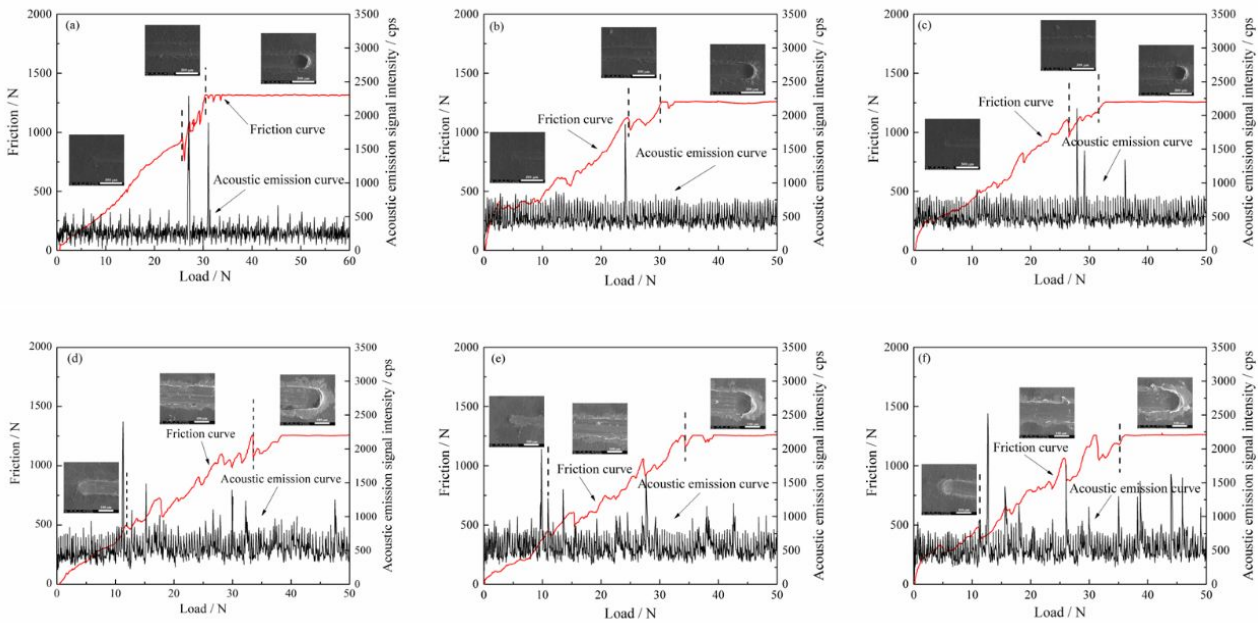


Fig. 7. Friction and acoustic signal curves of (a)–(c) CuHA/TiO₂-7.5min and (d)–(f) CuHA.

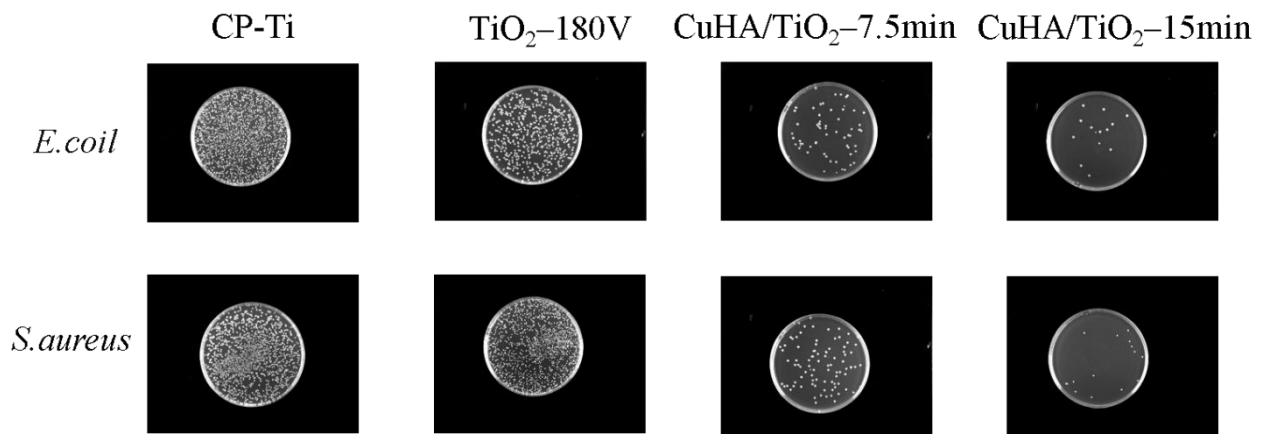


Fig. 8. Antibacterial properties of the samples against *E. coli* and *S. aureus*.

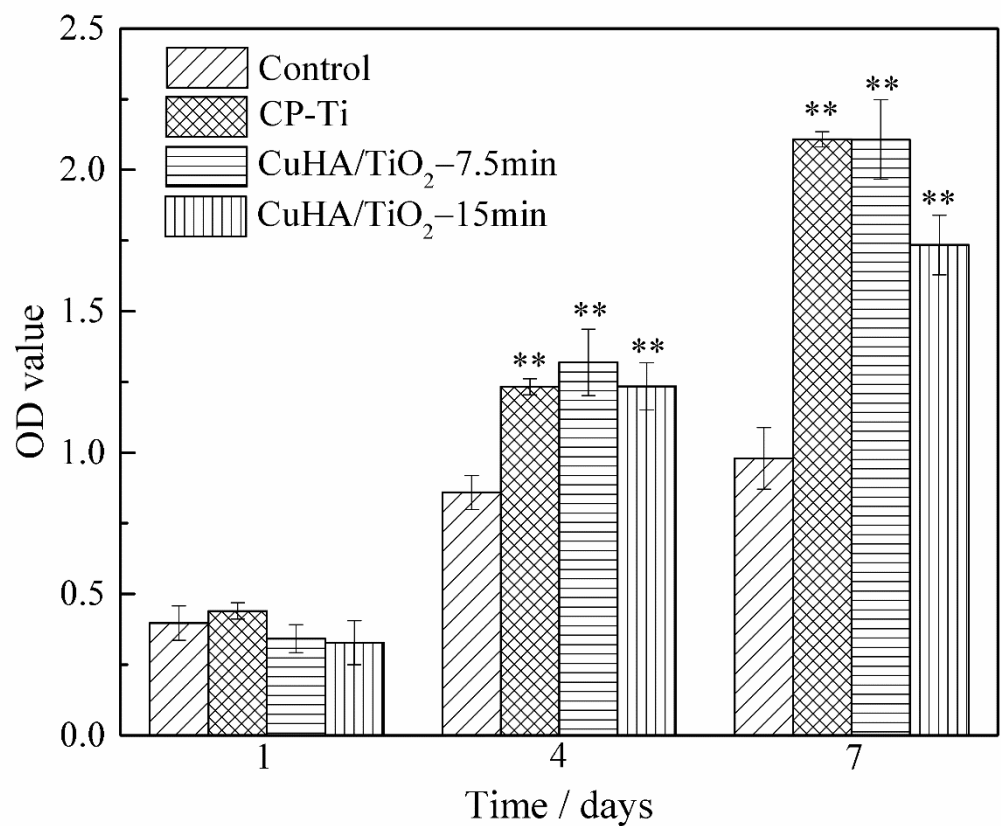


Fig. 9. Optical density values of MC3T3-E1 cells for the samples after culture for 1, 4, and 7 days. (** denotes a significant difference at P < 0.01 compared to the control)

Antibacterial Cu-doped HA/TiO₂ bioactive ceramic composite coating with enhanced adhesion on pure Ti

Jiawei Yang ¹, Qiang Li ^{1,2, *}, Junjie Li ³, Jinshuai Yang ¹, Ran Zhang ¹,

Mitsuo Niinomi ^{1,4,5,6,7 *}, Takayoshi Nakano ⁵

1. School of Mechanical Engineering, University of Shanghai for Science and Technology, Shanghai 200093, P. R. China

2. Shanghai Engineering Research Center of High-Performance Medical Device Materials, Shanghai 200093, P. R. China

3. CAS Key Laboratory of Functional Materials and Devices for Special Environments, Xinjiang Technical Institute of Physics & Chemistry, CAS; Xinjiang Key Laboratory of Electronic Information Materials and Devices, 40-1 South Beijing road, Urumqi 830011, P. R. China

4. Institute for Materials Research, Tohoku University, 2-1-1, Katahira, Aoba-ku, Sendai 980-8577, Japan

5. Division of Materials and Manufacturing Science, Graduate School of Engineering, Osaka University, 2-1, Yamada-Oka, Suita, Osaka 565-0871, Japan

6. Department of Materials Science and Engineering, Graduate School of Science and Technology, Meijo University, 1-501, Shiogamaguchi, Tempaku-ku, Nagoya 468-8502, Japan

7. Faculty of Chemistry, Materials and Bioengineering, Kansai University, Osaka 564-8680, Japan

* Corresponding authors:

Dr. Qiang Li, E-mail addresses: jxli@tju.edu.cn & liqiang@usst.edu.cn

Prof. Mitsuo Niinomi, E-mail address: niinomi@imr.tohoku.ac.jp

1
2
3
4
5
6
7
8
9
10
11
12
13
14
15
16
17
18
19
20
21
22
23
24
25
26
27
28
29
30
31
32
33
34
35
36
37
38
39
40
41
42
43
44
45
46
47
48
49
50
51
52
53
54
55
56
57
58
59
60

Abstract

Cu-doped hydroxyapatite (HA)/TiO₂ (CuHA/TiO₂) bioactive ceramic composite coatings were prepared on Ti surfaces using an electrochemical method to enhance their adhesion and antibacterial properties. The obtained coatings were characterized by scanning electron microscopy, X-ray diffraction, and X-ray photoelectron spectroscopy, while their adhesion was measured using a scratch ~~method~~test. The maximum adhesion between the TiO₂ layer and the substrate was 39.8 ± 2.6 N at an anodizing voltage of 180 V. Subsequently, the CuHA coatings were successfully deposited on the TiO₂ layers and grown outward along TiO₂ pores (during this process, Cu atoms ~~substituted Ca atoms~~ are doped into the HA structure in the form of Cu²⁺ ions). The CuHA adhesion to the TiO₂ layer was 26.3 ± 1.9 N, indicating that the TiO₂ interlayer significantly enhanced the bonding of CuHA to the substrate. Furthermore, the fabricated CuHA/TiO₂ coatings produced a strong antibacterial effect on *Escherichia coli* and *Staphylococcus aureus* species, exhibited high biocompatibility, and promoted the proliferation of MC3T3-E1 cells.

Keywords: TiO₂ nanopore, electrochemical deposition, Cu-doped hydroxyapatite coating, adhesion, antibacterial properties

1. Introduction

Ti and its alloys are widely used in biomedical implants, such as bone nails and artificial joints, because of their low density, excellent mechanical properties, and high biocompatibility (Ref 1, 2, 3, 4). However, Ti and its alloys are also biologically inert materials, ~~which that, on account of their~~ lack of biological activity, cannot promote the growth of bone tissues (Ref 5), and do not exhibit antibacterial properties, although bacterial infection and inflammation may occur after the long-term implantation of Ti-based materials into the human body (Ref 6). Therefore, the implant surface must be appropriately modified to enhance its osteogenic activity, adhesion, and antibacterial characteristics.

Hydroxyapatite (HA) is ~~the~~ main inorganic component of human bones that ~~can induce~~ induces the growth of new bones (Ref 7, 8). However, HA does not possess antibacterial properties, and its adhesion to Ti substrates is relatively weak (Ref 9, 10), which limits its clinical applications (Ref 11, 12). ~~In general, the good~~ Good adhesion between an HA coating and a Ti substrate is important but is often ignored in ~~the~~ clinical practice. Electrochemical deposition (ED) is an effective method for preparing HA coatings due to the easy control over the coating composition, low fabrication cost, high processing speed, and high coating purity (Ref 13). However, because this method covers the substrate surface with a ~~new~~ different material, the adhesion between the two components is relatively small. ~~Moreover, the crystallinity of HA coatings is very low (Ref 14), which results in their partial dissolution after implantation, decreasing the adhesion and ultimately causing a coating fall-off in vivo (Ref 15).~~ Say et al. (Ref ~~16~~ 14) have found that the addition of SiO₂ to ~~the coating~~ coatings produces a porous and crack-free surface morphology, which increases ~~its~~ adhesion and corrosion resistance while reducing the pore density. Yigit et al. (Ref ~~17, 18~~ 15, 16) have prepared nano-

hydroxyapatite-matrix coatings doped with different fractions of graphene nanosheets (GNS) on the Ti-6Al-7Nb and Ti-6Al-4V alloy surfaces by plasma electrolytic oxidation and a hydrothermal method. They found that both the coating porosity and HA crystallinity increased with an increase in the GNS content. TiO₂ has attracted widespread attention owing to its high corrosion resistance and ability to increase the bonding force between HA and the substrate (Ref [19, 2017, 18](#)). In particular, TiO₂ nanopores can considerably improve the adhesion properties of the substrate and provide a suitable living-environment for cell growth (Ref [19, 20, 21, 22, 23](#)). Dikici et al. (Ref [2422](#)) investigated the effects of rutile TiO₂ on a biphasic calcium phosphate (BCP) coating deposited on the β -type titanium alloy surface by a sol-gel method and. They observed that this coating increased the alloy-scratch and corrosion resistances. of the alloy. Anodic oxidization (AO) is a traditional surface modification method, which that can modify the chemical properties and structure of anodic films by varying different parameters such as applied voltage, electrolyte composition and concentration, and temperature (Ref [25, 2623, 24](#)). Therefore, it has become an attractive method for depositing oxide films on pure Ti surfaces. The results of multiple Multiple studies have revealed that an anatase or rutile TiO₂ film prepared by AO promoted the apatite formation in a simulated body fluid (Ref [27, 28, 29](#)). In recent years25, 26, 27). Recently, some metallic ions have been added to HA coatings to improve their antibacterial properties. A Zn-doped HA coating prepared by sol-gel and dip-coating methods was noncytotoxic and. It produced strong antibacterial effects on *Escherichia coli* (*E. coli*) and *Staphylococcus aureus* (*S. aureus*), but its antibacterial activity was very limited (Ref [30](#)). The28). Ag-doped calcium TiO₂ coatings prepared by the thermochemical treatment of Ti surfaces demonstrated high antibacterial activity (Ref [3129](#)). However, Ag is an expensive metal that exhibits some cytotoxicity, while; Ag atoms may diffuse into cells through the

“Trojan horse” mechanism and then release Ag^+ ions that negatively affect intracellular functions (Ref ~~32, 33~~30, 31). In contrast, Cu is an inexpensive metal with ~~strong~~excellent antibacterial ability. It ~~represents~~is an essential trace element for maintaining the function of mammalian cells and produces anabolic effects on bone metabolism (Ref ~~32, 33, 34, 35, 36, 37~~). Furthermore, the continuous release of trace amounts of Cu^{2+} ions can induce the formation of new bones (Ref ~~38~~36).

In a previous study, Cu-doped coatings with good antibacterial properties were prepared on Ti surfaces by ED (Ref ~~39~~37). In ~~this work~~the present study, to increase the adhesion between the coating and the substrate, an intermediate nanoporous TiO_2 layer was first deposited by AO, after which Cu-doped HA (CuHA) coatings were produced by ED. Finally, the surface properties, adhesion, antibacterial properties, and cytotoxicity of the fabricated composite coatings were determined by various techniques.

2. Experimental section

2.1. Sample preparation

Prior to electrochemical treatment, commercially pure Ti sheets (CP-Ti, purity: 99.5%) with sizes of $10 \times 10 \times 1 \text{ mm}^3$ were polished using 120–1200# SiC sandpaper and then ultrasonically cleaned with acetone, absolute ethanol, and distilled water for 15 min each. Subsequently, the Ti sheets were etched in a mixture of hydrofluoric and nitric acids with an $\text{HF}:\text{HNO}_3:\text{H}_2\text{O}$ volume ratio of 1:3:10 for 30 s. Finally, the sheets were ultrasonically cleaned in deionized water for 15 min and dried in a vacuum drying oven at 60°C .

To prepare a TiO_2 layer, two-electrode AO was carried out using direct current (Beijing Han Sheng Pu Yuan Technology Co., Ltd., HSPY-200-02) at constant voltages of 120, 150, and 180 V. This was

performed in a water bath at a temperature of 25 °C ~~and voltages of 120, 150, and 180 V for 1 min~~ using a Ti sheet as the anode, a platinum plate as the cathode, and a 2 mol/L H₂SO₄ solution as the electrolyte. The distance between cathodes and anodes was 2 cm. The obtained samples were ~~abbreviated~~termed as TiO₂–120V, TiO₂–150V, and TiO₂–180V, respectively.

After the AO process, a Cu-containing HA coating was deposited by ED in a water bath ~~set at a~~ ~~temperature of~~ 45 °C using a platinum sheet as the anode and the anodized sample as the cathode. The ~~utilized~~ electrolyte consisted of 0.040 mol/L CaCl₂·2H₂O, 0.025 mol/L NH₄H₂PO₄, and 0.001 mol/L CuCl₂·2H₂O, ~~and~~ Additionally, 0.1 mol/L NaCl, ~~which~~ was added to increase the solution conductivity. Samples were prepared at a constant voltage of 3 V for 7.5 and 15 min, after which they were ultrasonically cleaned with deionized water and dried in an oven at 60 °C. For convenience, the sample deposited for 7.5 min was ~~abbreviated~~termed as CuHA/TiO₂–7.5min, and the sample deposited for 15 min was ~~abbreviated~~labeled as CuHA/TiO₂–15min. For comparison, ~~a~~ ~~CuHA~~ ~~coating~~coatings without TiO₂ ~~was obtained~~were deposited on CP-Ti at a voltage of 3 V and deposition ~~timetimes~~ of 7.5 min and 15 min, which were termed as CuHA–7.5min and CuHA–15min, respectively.

2.2. Characterization techniques

Phase compositions and crystallinity were determined by X-ray diffraction (XRD, Bruker D8 Advance) with Cu K α radiation at a tube voltage of 40 kV, tube current of 40 mA, and scanning angles (2 θ) of 20°–80°. Surface morphologies were observed by scanning electron microscopy (SEM, FEI Quanta 450) at an accelerating voltage of 30 kV. Chemical compositions and elemental contents were analyzed by X-ray photoelectron spectroscopy (XPS, AIXS Ultra DLD) using a monochromatic

Al K α (h ν = 1486.6 eV) radiation source.

2.3. Adhesion test

The adhesion between the coating and the substrate was evaluated using an automatic scratch tester (Lanzhou Zhongke Kaihua Technology Development Co., Ltd., WS-2005), which contained a diamond indenter with a tip radius of 0.2 mm. Measurements were performed at an antenna angle of 120°, a load of 50 N, a load rate of 30 N/min, and a scratch length of 3 mm. Each sample was tested three times.

2.4. Evaluation of antibacterial properties

The antibacterial properties of the fabricated coatings were evaluated using *S. aureus* ATCC 29213 and *E. coli* ATCC 25922 cells. The number of colonies was measured by a plate counting method. TiO₂-180V, CuHA/TiO₂-7.5min, and CuHA/TiO₂-15min were subjected to antibacterial tests using CP-Ti as the control group. After sterilization in a high-temperature, high-pressure steam sterilizer for 20 min, the samples were added to a 24-well plate. The bacterial solution was diluted to 10⁶ CFU/mL with the Luria-Bertani (LB) liquid medium, and 0.2 mL of the diluted bacterial solution was added to the surface of a studied sample. Sterile normal saline was added to the empty ~~holes~~ wells to prevent water evaporation from the bacterial solution. The 24-well plate was placed in a constant-temperature incubator at 37 °C for 18 h. After the co-cultivation was complete, the co-culture solution was diluted to 10⁶ CFU/mL with a sterile phosphate-buffered saline (PBS) solution. ~~Afterwards~~ Afterward, 100 μ L of each diluted solution was evenly applied to the LB solid medium, which was then placed in a constant-temperature incubator at 37 °C for 18 h for static culture. At the

1
2
3
4
5
6
7
8
9
10
11
12
13
14
15
16
17
18
19
20
21
22
23
24
25
26
27
28
29
30
31
32
33
34
35
36
37
38
39
40
41
42
43
44
45
46
47
48
49
50
51
52
53
54
55
56
57
58
59
60

end of this process, the number of colonies was recorded. ~~Antibacterial~~The antibacterial rate was calculated via the following formula: antibacterial rate (%) = (CFU of the control sample – CFU of the tested sample) / CFU of the control sample × 100%.

2.5. Cytotoxicity test

MC3T3-E1 cells (iCell Bioscience Inc.) were used to evaluate the cytotoxicity of the produced coatings. The culture medium was α -MEM (Corning Inc.) supplemented with 10% fetal bovine serum (Biological Industries). CP-Ti, CuHA/TiO₂-7.5min, and CuHA/TiO₂-15min were selected for the cytocompatibility studies. ~~First, the~~The samples were first sterilized at high temperature and pressure. ~~Because they~~As the samples contained solid flakes, extraction was conducted at 37 °C for 24 h at a surface area/liquid volume ratio of 1.25 cm²/mL following the ISO10993-12 standard. Each sample extract (100 μ L) was placed into separate 96-well plates, and three parallel wells were set up for each sample. The MC3T3-E1 cells were inoculated into each well at densities of 2×10^3 cells/well for 1-d culturing and 1×10^3 cells/mL for 4-d and 7-d culturing. The 96-well plates were placed in a humidified incubator with a 5% CO₂ atmosphere for 1, 4, and 7 d at 37 °C. After culturing, each well was rinsed three times with PBS. The culture medium (100 μ L) with 10% MTT assay was added to each well and then incubated in a humidified incubator with a 5% CO₂ atmosphere for an additional 4 h at 37 °C. The supernatant was aspirated, and 100 μ L of dimethyl sulfoxide was added to each well, followed by gentle shaking for 10 min. Optical density (OD) was measured at a wavelength of 570 nm using a TECAN SPARK 10M enzyme-labeled instrument. As a control, MC3T3-E1 cells were directly seeded onto the bottoms of the wells without extracts.

3. Results and discussion

3.1. Adhesion properties of TiO₂ nanopores

The SEM images of the TiO₂ nanopores prepared at 120, 150, and 180 V are shown in Fig. 1. During the AO process, gas evolution and spark discharge occurred. After AO, a TiO₂ layer with a three-dimensional oxidation structure composed of numerous open pores was formed on the CP-Ti surface. Uniformly distributed nanopores with average sizes of approximately 100 nm were produced on the TiO₂-120V surface (Fig. 1a). The pores increased in size and became non-uniform as the voltage increased from 120 to 150 V (Fig. 1b). For TiO₂-180V, an alternating sequence of large and small holes was observed (Fig. 1c). The obtained XRD patterns (Fig. 2) ~~show~~showed that the TiO₂-120V sample mainly ~~consists~~consisted of Ti and anatase species, while TiO₂-150V ~~contains~~the contained Ti, anatase, and rutile components. The main phases of TiO₂-180V ~~are the~~were Ti and rutile ~~ones~~, and only a small peak corresponding to anatase ~~is~~was observed at 25.8°. It ~~was reported~~has been previously reported that a mixed structure of rutile and anatase TiO₂ exhibited high chemical stability and good mechanical properties (Ref 4038). Yang et al. have demonstrated that TiO₂ with specific anatase and rutile structures could induce apatite formation in vitro (Ref 4139). Additionally, rutile TiO₂ ~~promoted the~~has been reported to promote apatite deposition ~~of apatite~~ because of the lattice matching between the rutile and apatite phases (Ref 1540).

The scratch method was used to determine the adhesion between the TiO₂ layer and the substrate. The friction and acoustic signal curves of the samples prepared at different voltages are shown in Fig. 3. ~~When~~A sudden increase in the acoustic signal ~~suddenly increases, accompanied by a significant change in~~ the friction ~~is changed significantly. At this point, which occurs when~~ the coating is completely peeled off, ~~and the~~ The corresponding load is called a critical load. The adhesions of

TiO₂-120V, TiO₂-150V, and TiO₂-180V ~~are~~were equal to 32.2 ± 2.1 , 34.7 ± 2.5 , and 39.8 ± 2.6 N, respectively. Thus, the adhesion of the TiO₂ layer ~~increases~~increased with increasing voltage, which ~~is~~was likely due to the alternating sequence of ~~the~~ large and small holes. Such a multilevel structure facilitates mechanical interlocking and enhances coating adhesion. As the TiO₂-180V sample mainly consisted of rutile and exhibited the highest adhesion, the Cu-containing HA coatings were subsequently prepared on its surface.

3.2. Coating structure

The SEM images of the composite coatings are displayed in Fig. 4. Specifically, Fig. 4a shows that the nanopores are completely covered by dense flocculent crystals. After increasing the deposition time from 7.5 to 15 min, the crystals continued to aggregate and cluster together, producing a “community” distribution on the coating surface (Fig. 4b). ~~The corresponding XRD patterns (Fig. 5) contain typical HA peaks (JCPDS No. 72-1243) with a sharp peak at $2\theta \sim 26^\circ$ and the characteristic diffraction peaks of rutile TiO₂ and Ti. No other peaks were present in the XRD patterns~~Fig. 5 reveals the XRD patterns of Cu-doped HA coatings. In the figure, the diffraction peaks of HA are observed at the 2θ values of 25.9° , 28.1° , 32.2° , and 35.4° (JCPDS No. 09-0432) (Ref 37, 41). The characteristic diffraction peaks of Ti are also observed in all samples. For CuHA/TiO₂-7.5min and CuHA/TiO₂-15min, the rutile TiO₂ peaks appeared. The crystallinity of Cu-doped HA coatings is listed in Table 1. The crystallinity of the CuHA-7.5min and CuHA-15min coatings was $81.26 \pm 4.67\%$ and $80.12 \pm 4.27\%$, respectively. The addition of titanium dioxide reduced the crystallinity of CuHA/TiO₂-7.5min and CuHA/TiO₂-15min to $67.01 \pm 3.59\%$ and $64.82 \pm 3.55\%$, respectively. This is because TiO₂ is a semiconductor with lower electrical conductivity than that of pure titanium, which hinders the

electrochemical deposition process to a certain extent and inhibits the crystallization of HA.

The chemical compositions of the obtained samples measured by XPS are listed in Table 42. The Cu content in the coatings ~~increases~~increased from 1.44 to 2.53 ~~at.% with increasing% as~~ deposition time increased from 7.5 to 15 min. The full XPS profiles (Figs. 6a and c) indicate that the coatings mainly consisted of the elements Ca, P, Cu, O, C, and N ~~elements~~. The observed C peak is likely caused by the dissolved carbon dioxide in the electrolyte (Ref 3533). The high-resolution Cu spectra (Figs. 6b and d) contain ~~the~~ peaks with binding energies of 934.2 and 936.8 eV, corresponding to Cu–OH and Cu–PO₄ bonds, respectively (Ref 3937, 42), as well as ~~the~~ Cu²⁺ satellite peaks suggesting the presence of Cu atoms in the HA structure in the form of Cu²⁺ ions, which react with OH[–] and PO₄^{3–} ions. Thus, it can be concluded that Cu atoms ~~substituted Ca atoms in~~ are doped into the HA lattice ~~in the form of~~ Cu²⁺ ions.

3.3. Adhesion of composite coatings

The results of scratch testing demonstrated ~~the existence of~~ a relationship between the load, acoustic signal, and friction. ~~As shown in Fig. 7, friction~~Friction fluctuations are strongly related to the coating microstructure (Ref 43). ~~At high loads, the), which can be observed in Fig. 7. The~~ coating starts ~~to peel~~peeling off at high loads, as indicated by the observed scratch morphology. ~~According~~ As illustrated in Fig. 7a, the entire process, from the contact of the diamond indenter with the coating to the peeling of the coating, can be divided into three stages. ~~At~~In the first stage, the load is low; cracks begin to form inside the coating, and slight plastic deformation is observed on the coating surface. As a result, the ~~width of the~~ scratches on the coating surface ~~is~~are relatively narrow; further, the surface friction is low, and the acoustic emission signal value is stable. During the second stage,

the coating continues to plastically deform as the load further increases. After the diamond indenter scratches the coating, the rebound of the metal substrate produces transverse cracks on the coating surface, which span extend in different directions. When the load reaches a certain value, the friction factor between the substrate and the coating changes. Simultaneously, the noise generated when the coating is peeled off causes a sudden change in the acoustic emission signal (the corresponding load is called a critical load). After the coating is peeled off, the diamond indenter directly touches the substrate, and the friction increases with increasing load. During the third stage, when the load is equal to approximately 33 N, the friction reaches a maximum and then remains constant.

The As seen in Figs. 7a–c, the friction of the CuHA/TiO₂–7.5min composite coating was observed to suddenly decreases, and the strong noise leads to decrease along with a sudden rapid change in the acoustic emission signal at a load of approximately 26 N because the coating ~~becomes~~ completely peeled off ~~(the corresponding load is considered a critical load).~~ The adhesion of the CuHA/TiO₂–7.5min composite determined from the results of three different scratch tests ~~amounts to~~ was 26.3 ± 1.9 N. Similarly, the adhesion of the CuHA coating ~~is~~ was equal to 11.2 ± 1.4 N. Our findings compare favorably to those of Surmenev et al.; they prepared an HA coating by radio-frequency magnetron sputtering, which began to fall off at 5.5 N and was completely detached at a load of approximately 13.5 N (Ref 44). The adhesion of ~~the~~ a coating prepared by radio-frequency magnetron sputtering is usually higher than that of ~~the~~ a coating prepared via ED. However, in our work, the adhesion between HA and the substrate is relatively high owing to the presence of TiO₂ nanopores in the CuHA/TiO₂ composite coating, ~~the adhesion between HA and the substrate is relatively high.~~ Possible reasons for this phenomenon can be summarized as follows. (a) The Ti oxide particles present on the surface of the TiO₂ porous layer increase the coating roughness and adhesion (Ref 45).

(b) The OH^- ions on the surface of TiO_2 nanopores react to produce $\text{Ti}(\text{OH})_2 \cdot \text{H}_2\text{O}$ species, which form chemical bonds with the CuHA coating. The obtained Ti– TiO_2 –HA structure strengthens the bonds between the coating and the substrate (Ref 46). (c) The thermodynamic expansion coefficients of the CP-Ti and CuHA coatings are equal to $10.8 \times 10^{-6} / \text{K}$ and $15 \times 10^{-6} / \text{K}$, respectively. Their difference generates residual thermal stress and instantaneous thermal stress. The thermodynamic expansion coefficient of TiO_2 is $10.2 \times 10^{-6} / \text{K}$, which is close to that of CP-Ti. Thus, the residual stress generated by the mismatch between the thermodynamic expansion coefficients of the CuHA coating and CP-Ti substrate is buffered, ~~which inhibits~~inhibiting the formation of microcracks and effectively ~~reduces~~reducing the coating shedding probability (Ref 9, 47,48). (d) The CuHA coating begins to grow on the nanopore and forms ~~ana compact~~a compact CuHA/ TiO_2 -~~compact~~ layer with improved adhesion properties (Ref 45).

3.4. Antibacterial properties

Figure 8 depicts the colonies of *E. coli* and *S. aureus* after culturing at 37 °C for 24 h. For CP-Ti, numerous colonies are observed on the agar plate, which is consistent with the poor antibacterial property of Ti and its alloys (Ref 49). For TiO_2 -180V, the number of colonies is slightly reduced due to the limited antibacterial properties of this sample (its antibacterial rates for *E. coli* and *S. aureus* are only 26.8% and 23.1%, respectively). For the CuHA/ TiO_2 composite coatings, the number of colonies on the corresponding plates ~~are were~~ sharply reduced. The antibacterial rates of CuHA/ TiO_2 -7.5min for *E. coli* and *S. aureus* ~~are were~~ equal to 87% and 85%, respectively. Moreover, the antibacterial rates of CuHA/ TiO_2 -15min for the same cultures ~~amount to were~~ 96.1% and 95.8%, respectively. Therefore, both CuHA/ TiO_2 composite coatings exhibit strong antibacterial properties.

Note that the antibacterial properties of all coatings against *S. aureus* ~~are were~~ not as good as those against *E. coli* because the cell walls of *S. aureus* are thicker than the cell walls of *E. coli* (Ref 3533,50). With an increase in the Cu content, the antibacterial rate ~~increased~~ significantly ~~increases~~, which is consistent with the conclusions of Liu et al. (Ref 51). The ~~obtained~~ results clearly ~~demonstrated~~ ~~demonstrated~~ that the Cu-doped composite coatings ~~possess~~ ~~possessed~~ good antibacterial properties.

3.5. Cytotoxicity

The cytotoxicity of the CuHA/TiO₂ coatings was evaluated by conducting MTT tests using MC3T3-E1 as a cell model. As shown in Fig. 9, after 1 day of culture, the OD values of each group ~~remain~~ ~~remained~~ similar, and their differences ~~are were~~ not statistically significant. After 4 d, the OD values of all samples ~~increase~~ ~~increased~~, indicating that ~~their~~ ~~the~~ cells proliferate with increasing culture time. The OD values of the CP-Ti and CuHA/TiO₂ coatings ~~are were~~ ~~significantly~~ higher than that of the control group ~~with a statistically significant difference~~ ($P < 0.01$). However, the difference between these two samples ~~is was~~ not statistically significant. After 7 d of culture, the OD values of all groups further ~~increase~~ ~~increased~~, and no statistically significant difference between CP-Ti and CuHA/TiO₂-7.5min ~~are was~~ observed. The OD value of CuHA/TiO₂-15min ~~is was~~ much lower than those of CP-Ti and CuHA/TiO₂-7.5min, although it ~~is was~~ significantly higher than the OD of the control group, suggesting that CuHA/TiO₂-15min exhibits good cytocompatibility. The ~~obtained~~ results indicate that the Cu-doped HA/TiO₂ composite coatings demonstrate no cytotoxicity against osteoblast cells. However, excessive Cu amounts ~~considerably~~ ~~are known to~~ increase their cytotoxicity ~~considerably~~ (Ref 52). In this study, the Cu content ~~is was~~ maintained at a relatively low

level by adjusting the deposition time. The fabricated composite coatings ~~possess~~possessed enhanced adhesion and antibacterial properties without cytotoxicity; therefore, the proposed method is suitable for preparing antibacterial coatings.

4. Conclusion

In summary, novel antibacterial and biocompatible CuHA/TiO₂ composite coatings were prepared by AO combined with ED. The TiO₂ nanopores fabricated by AO at 180 V ~~exhibit~~exhibited good adhesion properties and ~~increase~~increased the adhesion of composite coatings when used as intermediate layers. During deposition, Cu atoms ~~substitute Ca atoms in~~were doped into the HA structure in the form of Cu²⁺ ions. The Cu content ~~increases~~increased from 1.44 to 2.53 at.% with ~~increasing an~~increase in deposition time from 7.5 to 15 min, while the Cu doping of HA significantly ~~enhances~~enhanced its antibacterial properties without exhibiting cytotoxicity. Thus, the proposed two-step ED method can be used ~~for improving~~to improve the adhesion and antibacterial properties of coated implants.

Acknowledgements

This work was partially supported by the Natural Science Foundation of Shanghai, China (No. 15ZR1428400), Shanghai Engineering Research Center of High-Performance Medical Device Materials (No. 20DZ2255500), and the Grant-in Aid for Scientific Research (C) (No. 20K05139) from JSPS (Japan Society for the Promotion of Science), Tokyo, Japan.

References

1. J. Wang, Y.A. Qing, L.G. Xiao, Y.G. Wang, X.F. Bao, Y.G. Qin, J.Y. Zhang, K. Zhang, Design of new-type F-FLC artificial joint coatings via fluorine incorporation and fullerene-like structure construction, *Surf. Coat. Tech.*, 2020, 385, p 125419, in English.
2. M. Pettersson, T. Berlind, S. Schmidt, S. Jacobson, L. Hultman, C. Persson, H. Engqvist, Structure and composition of silicon nitride and silicon carbon nitride coatings for joint replacements. *Surf. Coat. Tech.*, 2013, 235, p 827-834, in English.
3. M. Cuervas-Mons, E. León-Román, C. Solans, Á. Martínez-Ayora, J. Vaquero, Retrograde tibial nail and trabecular titanium spacer block for the treatment of missing talus: A Rare case report. *J. Foot Ankle Surg.*, 2020, 59(1), p 184-189, in English.
4. L. Korhonen, M. Perhomaa, A. Kyrö, T. Pokka, W. Serlo, J. Merikanto, J.-J. Sinikumpu, Intramedullary nailing of forearm shaft fractures by biodegradable compared with titanium nails: Results of a prospective randomized trial in children with at least two years of follow-up. *Biomaterials*, 2018, 185, p 383-392, in English.
5. A. Civantos, E. Martínez-Campos, V. Ramos, C. Elvira, A. Gallardo, A. Abarrategi, Titanium coatings and surface modifications: toward clinically useful bioactive implants. *ACS Biomater. Sci. Eng.*, 2017, 3(7), p 1245-1261, in English.
6. N.A. Hodges, E.M. Sussman, J.P. Stegemann, Aseptic and septic prosthetic joint loosening: Impact of biomaterial wear on immune cell function, inflammation, and infection. *Biomaterials*, 2021, 278, p 121127, in English.
7. L. Fathyunes, J. Khalil-Allafi, S.O.R. Sheykholeslami, M. Moosavifar, Biocompatibility assessment of graphene oxide-hydroxyapatite coating applied on TiO₂ nanotubes by ultrasound-assisted pulse electrodeposition. *Mat. Sci. Eng. C-Mater.*, 2018, 87, p 10-21, in English.

8. N. Karimi, M. Kharaziha, K. Raeissi, Electrophoretic deposition of chitosan reinforced graphene oxide-hydroxyapatite on the anodized titanium to improve biological and electrochemical characteristics. *Mat. Sci. Eng. C-Mater.*, 2019, 98, p 140-152, in English.
9. D.L. Qiu, L.J. Yang, Y.S. Yin, A.P. Wang, Preparation and characterization of hydroxyapatite/titania composite coating on NiTi alloy by electrochemical deposition. *Surf. Coat. Tech.*, 2011, 205(10), p 3280-3284, in English.
10. Z.J. Wu, L.P. He, Z.Z. Chen, Composite biocoating of hydroxyapatite/ Al_2O_3 on titanium formed by Al anodization and electrodeposition. *Mater. Lett.*, 2007, 61(14-15), p 2952-2955, in English.
11. L. Suo, N. Jiang, Y. Wang, P.Y. Wang, J.Y. Chen, X.B. Pei, J. Wang, Q.B. Wan, The enhancement of osseointegration using a graphene oxide/chitosan/hydroxyapatite composite coating on titanium fabricated by electrophoretic deposition. *J. Biomed. Mater. Res. B*, 2019, 107, p 635-645, in English.
12. Y.H. Duan, S. Zhu, F. Gao, J.Y. Zhu, M. Li, J. Ma, Q.S. Zhu, The effect of adhesive strength of hydroxyapatite coating on the stability of hydroxyapatite-coated prostheses in vivo at the early stage of implantation. *Arch. Med. Sci.*, 2012, 8, p 199-208, in English.
13. M. Hadidi, A. Bigham, E. Saebnoori, S.A. Hassanzadeh-Tabrizi, S. Rahmati, Z.M. Alizadeh, V. Nasirian, M. Rafienia, Electrophoretic-deposited hydroxyapatite-copper nanocomposite as an antibacterial coating for biomedical applications. *Surf. Coat. Tech.*, 2017, 321, p 171-179, in English.
14. Y. Say, B. Aksakal, B. Dikici, D.H. He, X.X. Zhang, P. Liu, X.K. Liu, X.H. Chen, F.C. Ma, W. Li, K. Zhang, H.L. Zhou, Effect of ~~hydrothermal treatment temperature on the~~ hydroxyapatite/ SiO_2 ~~hybride~~ coatings ~~deposited by electrochemical method~~. *Surf. Coat. Tech.*, 2021, 406(1 on surface morphology and corrosion resistance of REX-734 alloy. *Ceram. Int.*, 2016, 42(8), p 12665610151-

[10158](#), in English.

~~1515. S. Ban, S. Maruno, A. Harada, M. Hattori, K. Narita, J. Hasegawa, Effect of temperature on morphology of electrochemically deposited calcium phosphates. Dent. Mater. J., 1996, 15(1), p 31-38, in English.~~

~~16. Y. Say, B. Aksakal, B. Dikici, Effect of hydroxyapatite/SiO₂ hybride coatings on surface morphology and corrosion resistance of REX-734 alloy. Ceram. Int., 2016, 42(8), p 10151-10158, in English.~~

17. O. Yigit; N. Ozdemir, B. Dikici, M. Kaseem, Surface Properties of Graphene Functionalized TiO₂/nHA Hybrid Coatings Made on Ti6Al7Nb Alloys via Plasma Electrolytic Oxidation (PEO). Molecules, 2021, 26(13), p 3903, in English.

~~18~~16. O. Yigit, B. Dikici, T.C. Senocak, N. Ozdemir, One-step synthesis of nano-hydroxyapatite/graphene nanosheet hybrid coatings on Ti6Al4V alloys by hydrothermal method and their in-vitro corrosion responses. Surf. Coat. Tech., 2020, 394, p 125858, in English.

~~19~~17. Y. Wu, Q.Q. Li, B.Y. Xu, H.Y. Fu, Y. Li, Nano-hydroxyapatite coated TiO₂ nanotubes on Ti-19Zr-10Nb-1Fe alloy promotes osteogenesis in vitro. Colloids Surf. B, 2021, 207, p 112019, in English.

~~20~~18. X.J. Long, L. Duan, W.J. Weng, K. Cheng, D.P. Wang, H.W. Ouyang, Light-induced osteogenic differentiation of BMSCs with graphene/TiO₂ composite coating on Ti implant. Colloids Surf. B, 2021, 207, p 111996, in English.

~~21~~19. X. Cui, H.-M. Kim, M. Kawashita, L. Wang, T. Xiong, T. Kokubo, T. Nakamura, Preparation of bioactive titania films on titanium metal via anodic oxidation. Dent. Mater., 2009, 25(1), p 80-86, in English.

- [2220](#). S. Khanmohammadi, M. Ojaghi-Ilkhchi, M. Farrokhi-Rad, Development of bioglass coating reinforced with hydroxyapatite whiskers on TiO₂ nanotubes via electrophoretic deposition. *Ceram. Int.*, 2021, 47(1), p 1333-1343, in English.
- [2321](#). B. Feng, X.J. Chu, J.M. Chen, J.X. Wang, X. Lu, J. Weng, Hydroxyapatite coating on titanium surface with titania nanotube layer and its bond strength to substrate. *J. Porous Mater.*, 2010, 17(4), p 453-458, in English.
- [2422](#). B. Dikici, M. Niinomi, M. Topuz, S.G. Koc, M. Nakai, Synthesis of biphasic calcium phosphate (BCP) coatings on β -type titanium alloys reinforced with rutile-TiO₂ compounds: adhesion resistance and in-vitro corrosion. *J. Sol-Gel Sci. Technol.* 2018, 87, p 713–724, in English.
- [2523](#) Y.-T. Sul, C.B. Johansson, S. Petronis, A. Krozer, Y. Jeong, A. Wennerberg, T. Albrektsson, Characteristics of the surface oxides on turned and electrochemically oxidized pure titanium implants up to dielectric breakdown: the oxide thickness, micropore configurations, surface roughness, crystal structure and chemical composition. *Biomaterials*, 2002, 23(2), p 491-501, in English.
- [2624](#). Y.-T. Sul, C.B. Johansson, Y. Jeong, T. Albrektsson, The electrochemical oxide growth behaviour on titanium in acid and alkaline electrolytes. *Med. Eng. Phys.*, 2001, 23(5), p 329-346, in English.
- [2725](#). X.l. Zhu, K.-H. Kim, Y. Jeong, Anodic oxide films containing Ca and P of titanium biomaterial. *Biomaterials*, 2001, 22(16), p 2199-2206, in English.
- [2826](#). D. Velten, V. Biehl, F. Aubertin, B. Valeske, W. Possart, J. Breme, Preparation of TiO₂ layers on cp-Ti and Ti6Al4V by thermal and anodic oxidation and by sol-gel coating techniques and their characterization. *J. Biomed. Mater. Res.*, 2002, 59(1), p 18-28, in English.
- [2927](#). R. Rohanizadeh, M. Al-Sadeq, R.Z. Legeros, Preparation of different forms of titanium oxide

on titanium surface: effects on apatite deposition. *J. Biomed. Mater. Res. A*, 2004, 71(2), p 343-352.
in English.

[3028](#). Q. Bi, X. Song, Y.J. Chen, Y.P. Zheng, P. Yin, T. Lei, Zn-HA/Bi-HA biphasic coatings on Titanium: Fabrication, characterization, antibacterial and biological activity. *Colloids Surf. B*, 2020, 189, p 110813, in English.

[3129](#). A. Rodríguez-Contreras, D. Torres, B. Rafik, M. Ortiz-Hernandez, M.P. Ginebra, J.A. Calero, J.M. Manero, E. Ruperez, Bioactivity and antibacterial properties of calcium- and silver-doped coatings on 3D printed titanium scaffolds. *Surf. Coat. Tech.*, 2021, 421, p 127476, in English.

[3230](#). H. Hu, W. Zhang, Y. Qiao, X. Jiang, X. Liu, C. Ding, Antibacterial activity and increased bone marrow stem cell functions of Zn-incorporated TiO₂ coatings on titanium. *Acta Biomater.*, 2012, 8(2), p 904-915, in English.

[3331](#). E.-J. Park, J. Yi, Y. Kim, K. Choi, K. Park, Silver nanoparticles induce cytotoxicity by a Trojan-horse type mechanism. *Toxicol. In Vitro*, 2010, 24(3), p 872-878, in English.

[3432](#). M. Thukkaram, M. Vaidulych, O. Kylián, P. Rigole, S. Aliakbarshirazi, M. Asadian, A. Nikiforov, H. Biederman, T. Coenye, G.D. Laing, R. Morent, A.V. Tongel, L.D. Wilde, K. Verbeken, N.D. Geyter, Biological activity and antimicrobial property of Cu/a-C:H nanocomposites and nanolayered coatings on titanium substrates. *Mat. Sci. Eng. C-Mater.*, 2021, 119, p 111513, in English.

[3533](#). H.B. Wu, X.Y. Zhang, Z.H. Geng, Y. Yin, R.Q. Hang, X.B. Huang, X.H. Yao, B. Tang, Preparation, antibacterial effects and corrosion resistant of porous Cu–TiO₂ coatings. *Appl. Surf. Sci.*, 2014, 308, p 43-49, in English.

[3634](#). A. Hoppe, N.S. Güldal, A.R. Boccaccini, A review of the biological response to ionic dissolution products from bioactive glasses and glass-ceramics. *Biomaterials*, 2011, 32(11), p 2757-

2774, in English.

[3735](#). I. Burghardt, F. Lüthen, C. Prinz, B. Kreikemeyer, C. Zietz, H.-G. Neumann, J. Rychly, A dual function of copper in designing regenerative implants. *Biomaterials*, 2015, 44, p 36-44, in English.

[3836](#). N.J. Lakhkar, I.-H. Lee, H.-W. Kim, V. Salih, I.B. Wall, J.C. Knowles, Bone formation controlled by biologically relevant inorganic ions: Role and controlled delivery from phosphate-based glasses. *Adv. Drug. Delivery Rev.*, 2013, 65(4), p 405-420, in English.

[3937](#). Q. Li, J.S. Yang, J.J. Li, R. Zhang, M. Nakai, M. Niinomi, T. Nakano, Antibacterial Cu-doped calcium phosphate coating on pure titanium. *Mater. Trans.*, 2021, 62(7), p 1052-1055, in English.

[4038](#). F. Hilario, V. Roche, R.P. Nogueira, A.M.J. Junior, Influence of morphology and crystalline structure of TiO₂ nanotubes on their electrochemical properties and apatite-forming ability. *Electrochim. Acta*, 2017, 245, p 337-349, in English.

[4139](#). B.C. Yang, M. Uchida, H.-M. Kim, X.D. Zhang, T. Kokubo, Preparation of bioactive titanium metal via anodic oxidation treatment. *Biomaterials*, 2004, 25(6), p 1003-1010, in English.

[40](#). S. Ban, S. Maruno, A. Harada, M. Hattori, K. Narita, J. Hasegawa, Effect of temperature on morphology of electrochemically-deposited calcium phosphates. *Dent. Mater. J.*, 1996, 15(1), p 31-38, in English.

[41](#). L. Ling, T.T. Li, M.C. Lin, Q. Jiang, H.T. Ren, C.W. Lou, J.H. Lin, Effect of hydrogen peroxide concentration on the nanostructure of hydroxyapatite coatings via ultrasonic-assisted electrodeposition. *Mater. Lett.*, 2020, 261, p 126989, in English.

42. M.C. Biesinger, Advanced analysis of copper X-ray photoelectron spectra. *Surf. Interface Anal.*, 2017, 49(13), p 1325-1334, in English.

43. H. Pelletier, A. Carrado, J. Faerber, I.N. Mihailescu, Microstructure and mechanical

characteristics of hydroxyapatite coatings on Ti/TiN/Si substrates synthesized by pulsed laser deposition. *Appl. Phys. A*, 2011, 102(3), p 629-640, in English.

44. R.A. Surmenev, I.Y. Grubova, E. Neyts, A.D. Teresov, N.N. Koval, M. Epple, A.I. Tyurin, V.F. Pichugin, M.V. Chaikina, M.A. Surmeneva, Ab initio calculations and a scratch test study of RF-magnetron sputter deposited hydroxyapatite and silicon-containing hydroxyapatite coatings. *Surf. Interfaces*, 2020, 21, p 100727, in English.

45. S. Ahmadi, I. Mohammadi, S.K. Sadrnezhad, Hydroxyapatite based and anodic Titania nanotube biocomposite coatings: Fabrication, characterization and electrochemical behavior. *Surf. Coat. Tech.*, 2016, 287, p 67-15, in English.

46. C.-M. Lin, S.-K. Yen, Characterization and bond strength of electrolytic HA/TiO₂ double layers for orthopedic applications. *J. Mater. Sci.-Mater. M.*, 2004, 15(11), p 1237-1246, in English.

47. H. Farnoush, J.A. Mohandesi, H. Çimenoglu, Micro-scratch and corrosion behavior of functionally graded HA-TiO₂ nanostructured composite coatings fabricated by electrophoretic deposition. *J. Mech. Behav. Biomed.*, 2015, 46, p 31-40, in English.

48. W.J. Weng, S. Zhang, K. Cheng, H.B. Qu, P.Y. Du, G. Shen, J. Yuan, G.R. Han, Sol-gel preparation of bioactive apatite films. *Surf. Coat. Tech.*, 2003, 167(2-3), p 292-296, in English.

49. S.L. Mei, H.Y. Wang, W. Wang, L.P. Tong, H.B. Pan, C.S. Ruan, Q.L. Ma, M.Y. Liu, H.L. Yang, L. Zhang, Y.C. Cheng, Y.M. Zhang, L.Z. Zhao, P.K. Chu, Antibacterial effects and biocompatibility of titanium surfaces with graded silver incorporation in titania nanotubes. *Biomaterials*, 2014, 35(14), p 4255-4265, in English.

50. N. Murugan, C. Murugan, A.K. Sundramoorthy, In vitro and in vivo characterization of mineralized hydroxyapatite/polycaprolactone-graphene oxide based bioactive multifunctional

coating on Ti alloy for bone implant applications. *Arabian J. Chem.*, 2018, 11(6), p 959-969, in English.

51. J. Liu, F.B. Li, C. Liu, H.Y. Wang, B.R. Ren, K. Yang, E.L. Zhang, Effect of Cu content on the antibacterial activity of titanium–copper sintered alloys. *Mat. Sci. Eng. C-Mater.*, 2014, 35(1), p 392-400, in English.

52. R.Q. Hang, A. Gao, X.B. Huang, X.G. Wang, X.Y. Zhang, L. Qin, B. Tang, Antibacterial activity and cytocompatibility of Cu-Ti-O nanotubes. *J. Biomed. Mater. Res. A*, 2014, 102(6), p 1850-1858, in English.

For Peer Review

1
2
3
4
5
6
7
8
9
10
11
12
13
14
15
16
17
18
19
20
21
22
23
24
25
26
27
28
29
30
31
32
33
34
35
36
37
38
39
40
41
42
43
44
45
46
47
48
49
50
51
52
53
54
55
56
57
58
59
60

Table 1. Crystallinity of Cu-doped HA coatings.

<u>Sample</u>	<u>CuHA–7.5min</u>	<u>CuHA–15min</u>	<u>CuHA/TiO₂–7.5min</u>	<u>CuHA/TiO₂–15min</u>
<u>Crystallinity</u>	<u>81.26 ± 4.67%</u>	<u>80.12 ± 4.27%</u>	<u>67.01 ± 3.59%</u>	<u>64.82 ± 3.55%</u>

Table 2. Chemical compositions (at.%) of the samples measured by XPS.

<u>Sample</u>	<u>Ti</u>	<u>O</u>	<u>Cu</u>	<u>P</u>	<u>Ca</u>
CuHA/TiO ₂ –7.5min	0.02 ± 0.17	66.25 ± 0.46	1.44 ± 0.27	15.05 ± 0.39	17.33 ± 0.26
CuHA/TiO ₂ –15min	0.01 ± 0.10	66.19 ± 0.43	2.53 ± 0.27	15.11 ± 0.33	16.16 ± 0.25

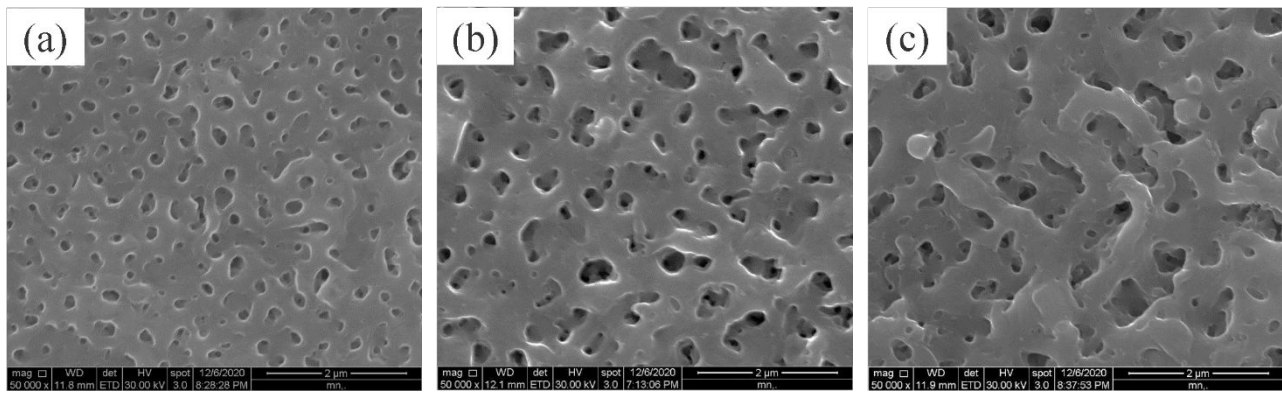


Fig. 1. SEM images of (a) TiO_2 -120V, (b) TiO_2 -150V, and (c) TiO_2 -180V.

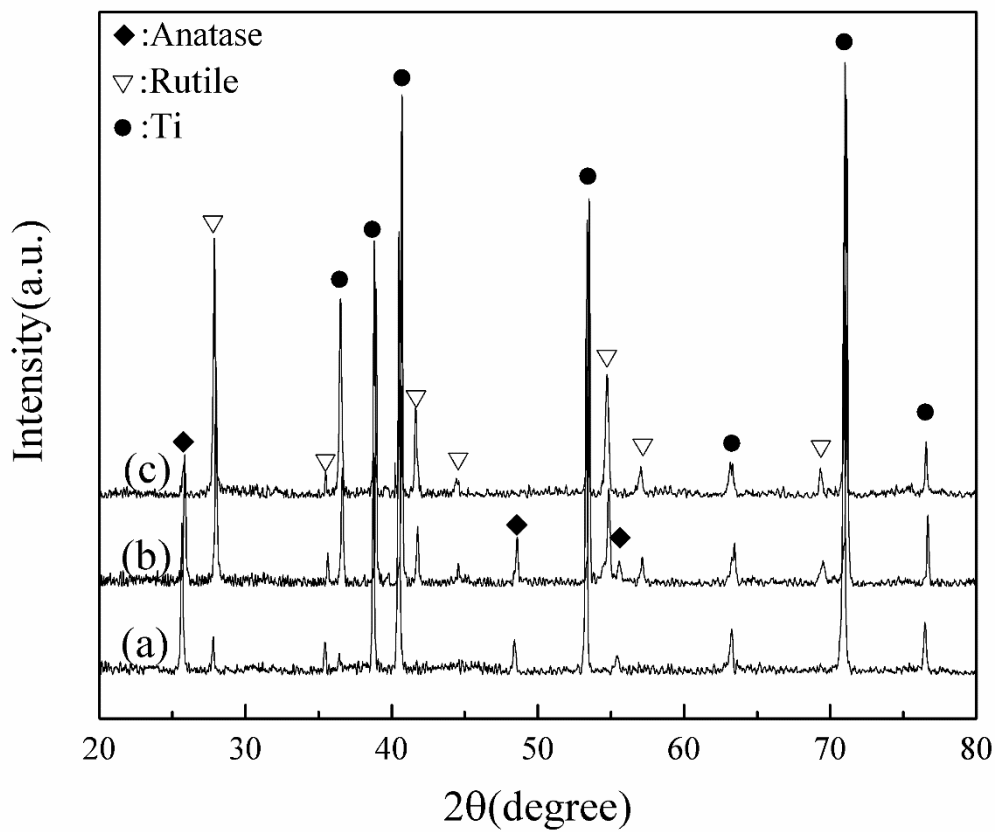


Fig. 2. XRD patterns of (a) TiO_2 -120V, (b) TiO_2 -150V, and (c) TiO_2 -180V.

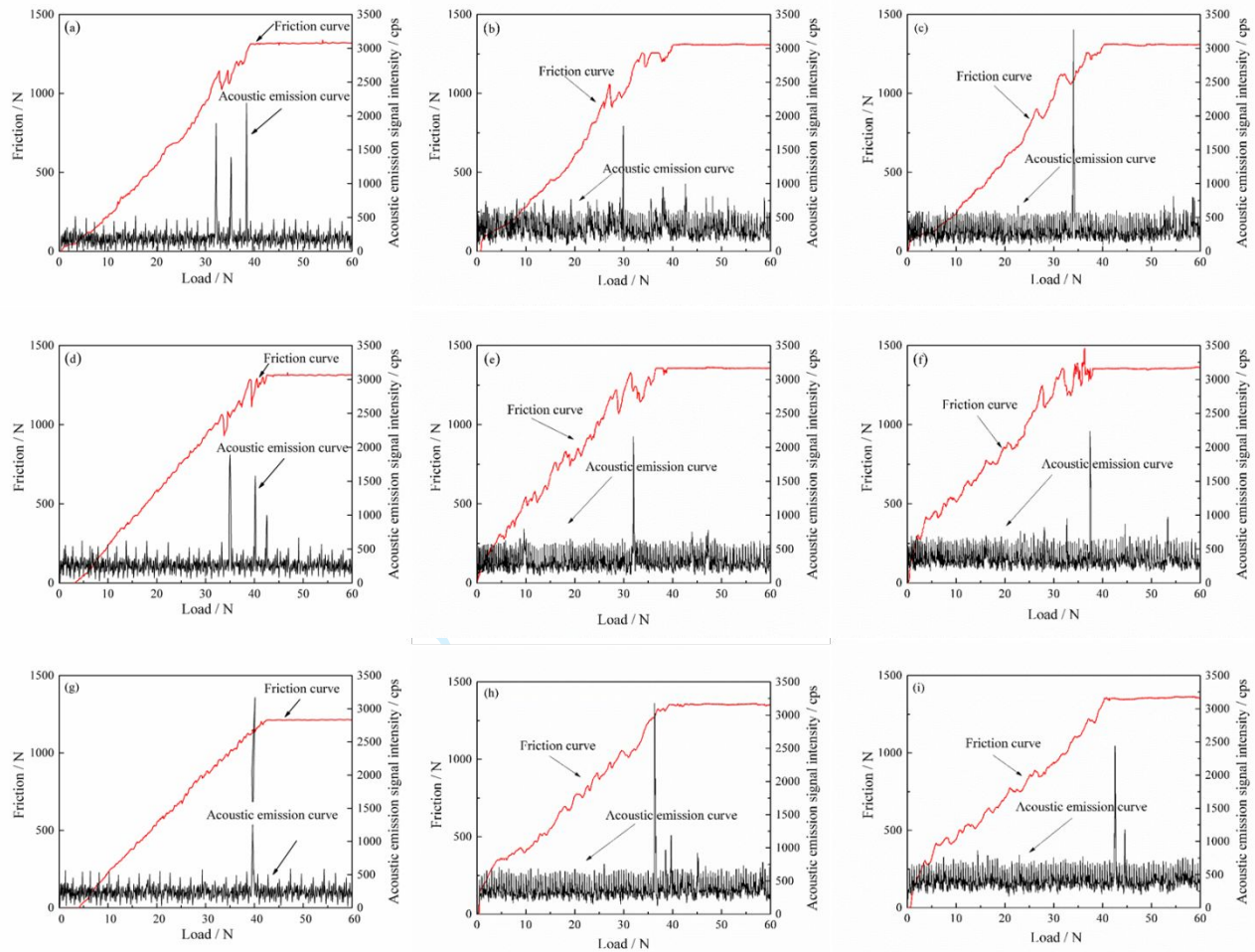


Fig. 3. Friction and acoustic signal curves of (a)–(c) TiO_2 –120V, (d)–(f) TiO_2 –150V, and (g)–(i) TiO_2 –180V.

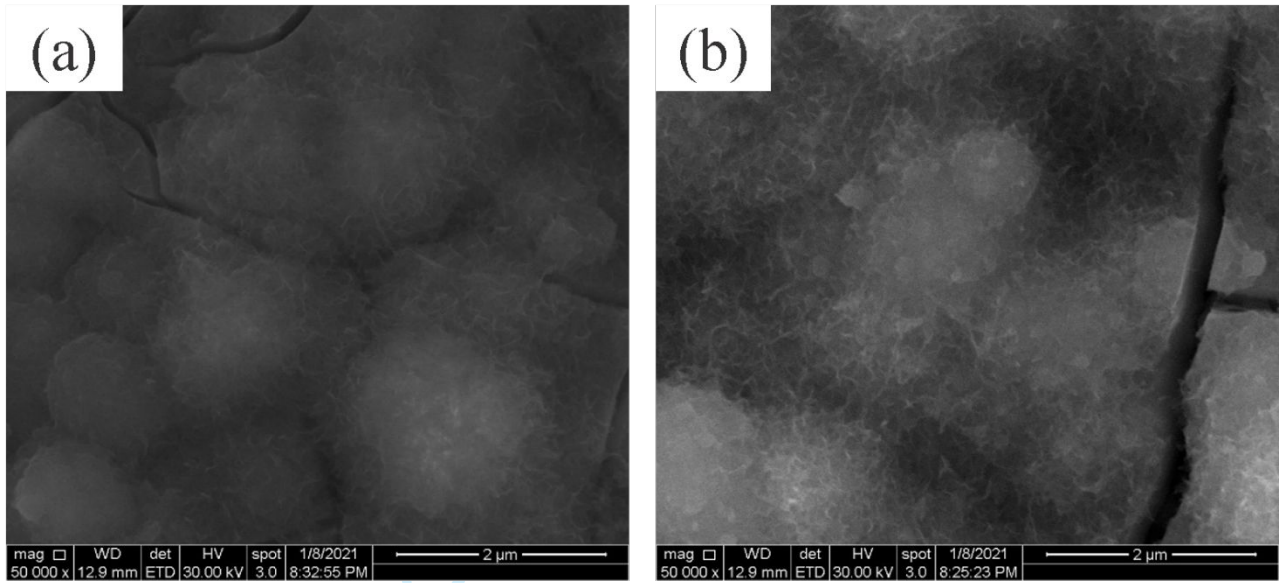
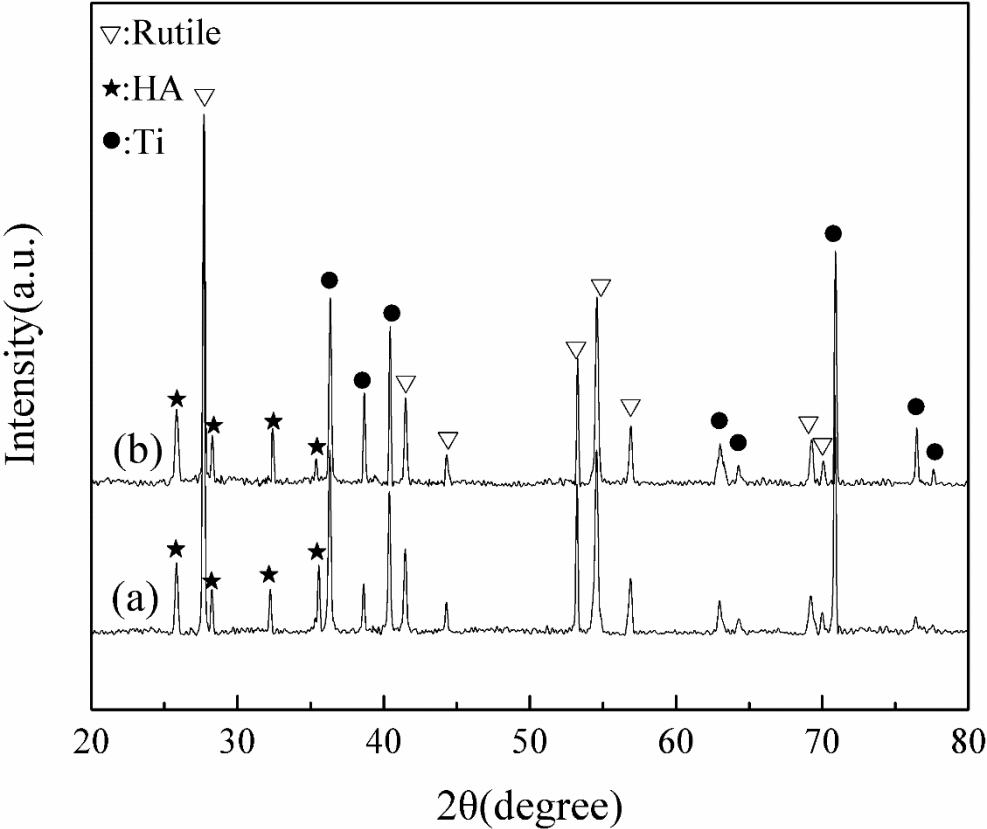


Fig. 4. SEM images of (a) CuHA/TiO₂–7.5min and (b) CuHA/TiO₂–15min.



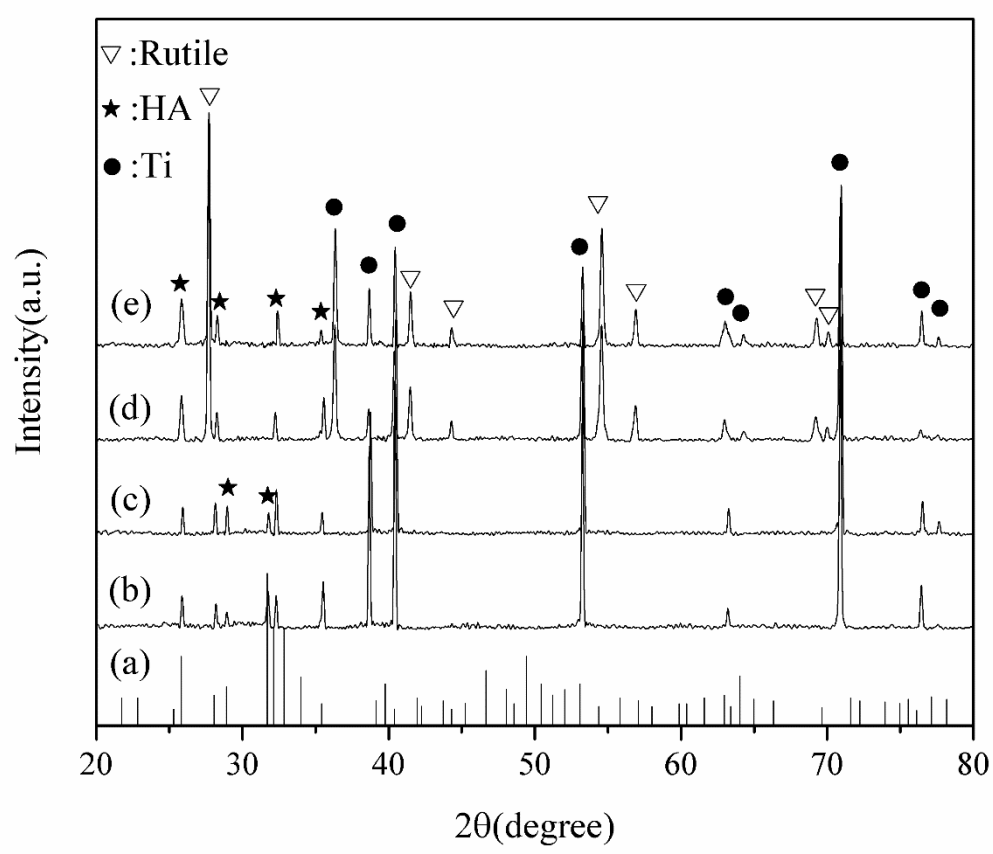


Fig. 5. (a) HA pattern ICCD 09-0432 and XRD patterns of (a)-b) CuHA-7.5min, (c) CuHA-15min, (d) CuHA/TiO₂-7.5min, and (e) CuHA/TiO₂-15min.

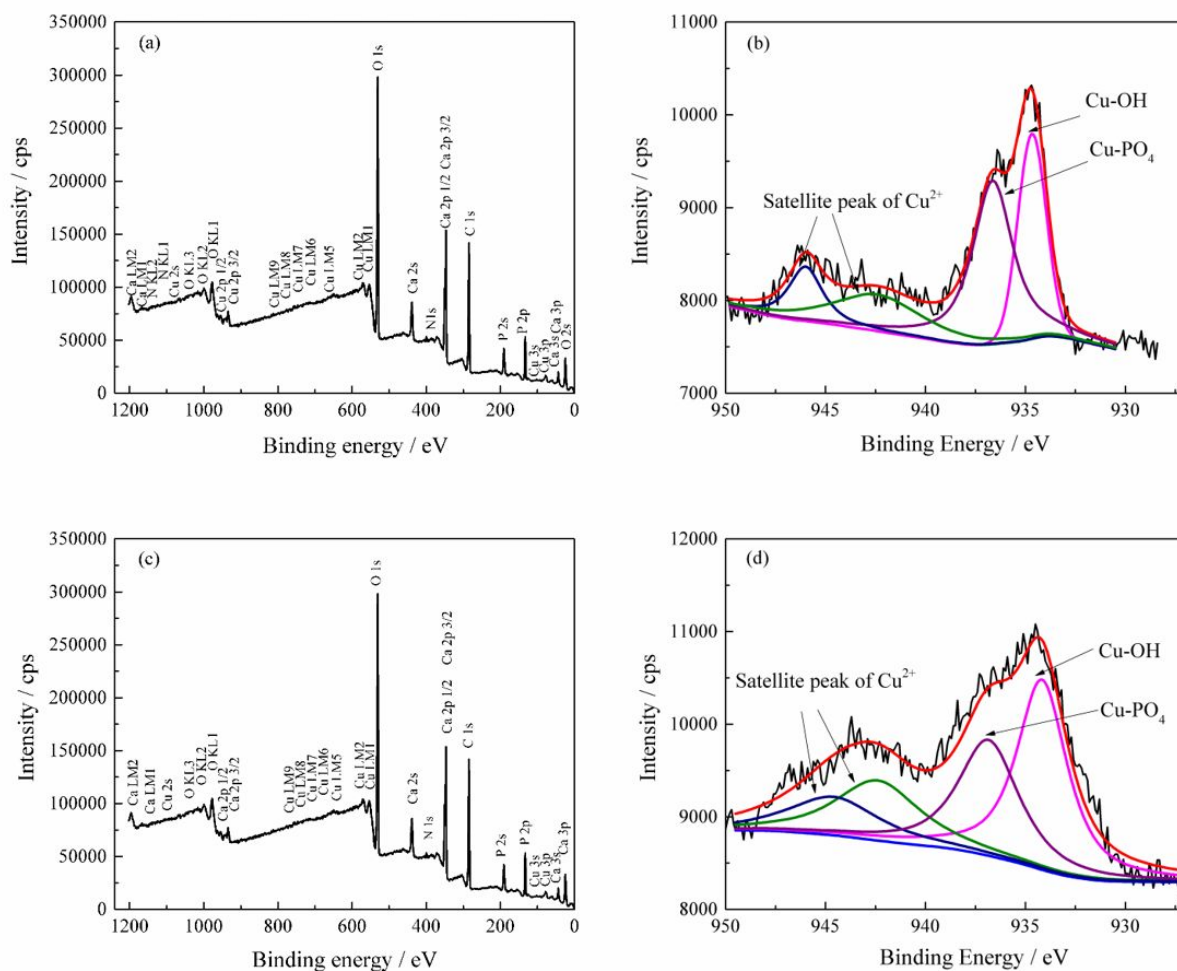


Fig. 6. XPS survey spectra (a, c) and Cu 2p high-resolution spectra (b, d) of (a) (b) CuHA/TiO₂–7.5min and (c) (d) CuHA/TiO₂–15min.

1
2
3
4
5
6
7
8
9
10
11
12
13
14
15
16
17
18
19
20
21
22
23
24
25
26
27
28
29
30
31
32
33
34
35
36
37
38
39
40
41
42
43
44
45
46
47
48
49
50
51
52
53
54
55
56
57
58
59
60

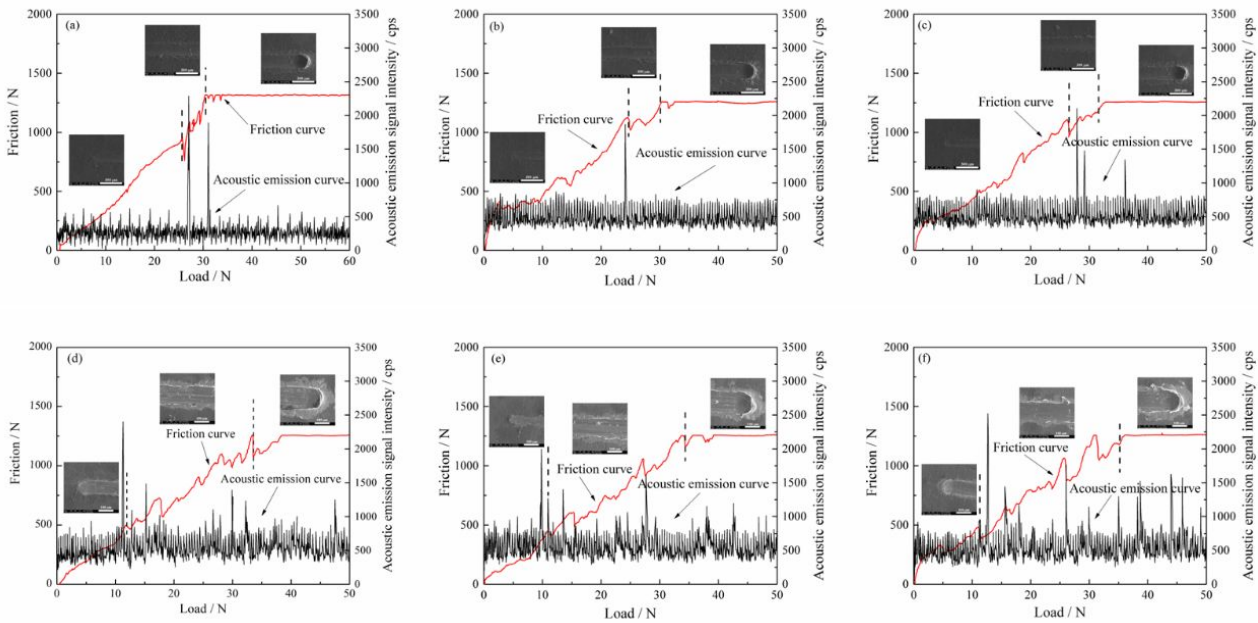


Fig. 7. Friction and acoustic signal curves of (a)–(c) CuHA/TiO₂-7.5min and (d)–(f) CuHA.

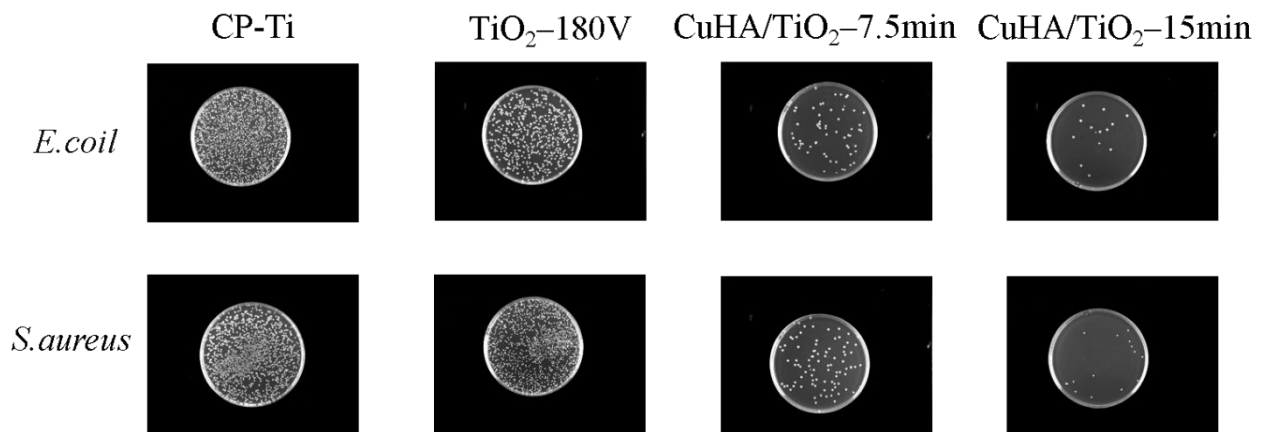


Fig. 8. Antibacterial properties of the samples against *E. coli* and *S. aureus*.

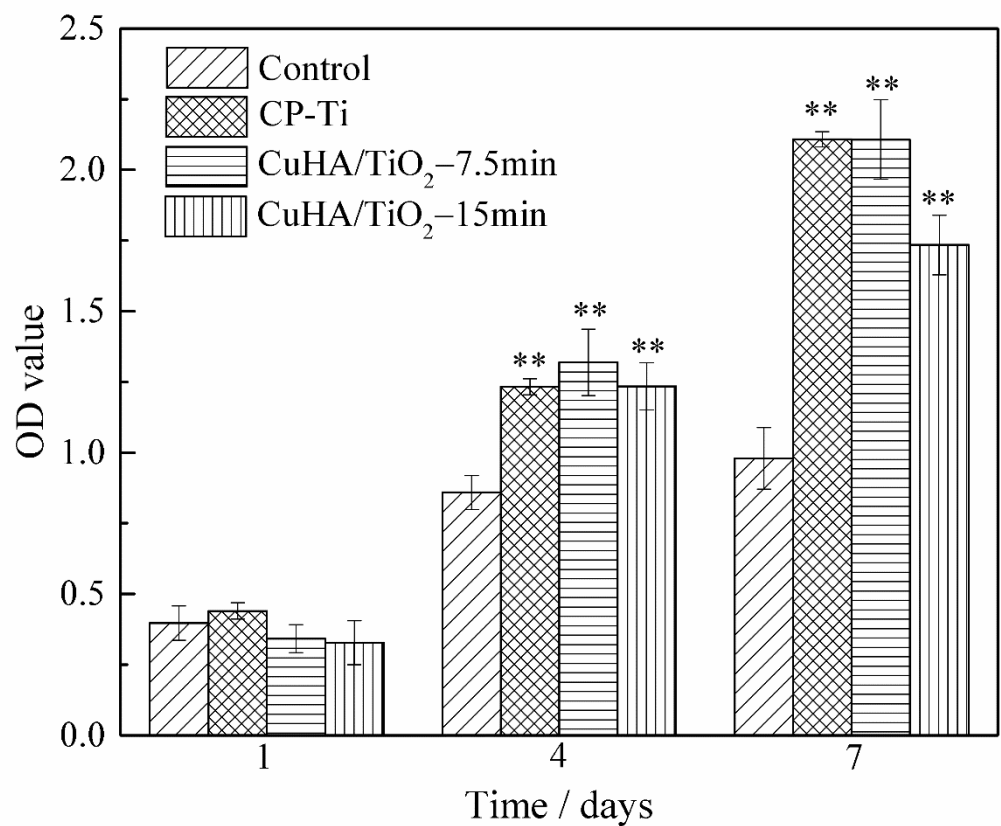


Fig. 9. Optical density values of MC3T3-E1 cells for the samples after culture for 1, 4, and 7 days culture. (** denotes a significant difference at P < 0.01 compared to the control)